

1 Response to Referee # 1

2
3 **RC: Referee's comment**

4 **AR: Author's response**

5
6 The referee is encouraged to refer our response to comments and concerns raised by the
7 anonymous referee # 2, where we have incorporated additional analysis to the manuscript.

8
9 RC: The paper is very interesting because it is the first time a comparison study is performed
10 using a large number of SKYNET sites and products from this network. In addition, the results
11 are very important for the developers of Skyrad pack improvements, particularly for what
12 concern the assumption of fixed value of Surface Albedo.

13 AR: We appreciate the reviewer for the constructive comments. In the OMI-SKYNET
14 comparison, we have considered all SKYNET stations whose data are freely accessible online
15 from Chiba University SKYNET server. As the referee as stated here, the purpose of such
16 comparison, particularly when both quantities are not directly measured but retrieved using
17 respective algorithms, is to understand and diagnose the (dis)agreement between the two
18 datasets to improve the accuracy of both retrievals.

19
20 RC: Lines: 65-66: specify if the change of estimated radiative forcing refers to the top, bottom
21 or middle atmosphere.

22 AR: The sentence is modified as "Together, both AOD and SSA determine the magnitude and
23 sign of the aerosol radiative forcing at the top-of-atmosphere."

24
25 RC: Line 170: both the POMs models take also measurements at 315 and 940 nm for Ozone and
26 water vapour retrieval. Add this information here and in line 178.

27 AR: The header information given in both POM-01 and POM-02 datasets states that the former
28 sensor carries a total of five wavelength filters covering visible to near-IR (400-1020 nm),
29 whereas the latter has two additional filters in the UV region (340 and 380 nm) along with the
30 other filters in the visible to shortwave-IR (including 1627 nm and 2200 nm) part of the
31 spectrum. These data files do not mention the use of 315 and 940 nm for Ozone and water
32 vapor retrievals.

33
34 RC: Line 186: remove and between University and Valencia

35 AR: Corrected.

36
37 RC: Line 255: add "carbonaceous/smoke"

38 AR: Corrected.

39
40 RC: Lines 255-257: it not clear to me according to which parameter has been considered the 5
41 listed sites better than the others. Moreover looking at Figure 2 the largest percentage of
42 agreement is for Q_0.05 and not 0.03.

43 AR: The sentence referred here is for the carbonaceous/smoke aerosol type (red dots in the
44 scatterplots), for which the majority of matchups are confined within the difference of 0.03. For

45 the overall comparison between the sites, we considered RMSD and % matchups falling within
46 0.03/0.05 as criteria. Lower RMSD and higher % matchups (Q_0.03 & Q_0.05) suggest a better
47 comparison between OMI and SKYNET SSAs.

48

49 RC: Line 348, it is better specify that the assumption of fixed ground albedo in Skyrad pack can
50 be changed in time and wavelengths, if necessary. For example in ESR/SKYNET, Antarctica sites
51 are processed with different values.

52 AR: The first two sentences are revised as “The standard SKYNET inversion algorithm assumes a
53 wavelength-independent surface albedo of 0.1 at all wavelengths across the UV to visible part
54 of the spectrum. However, the algorithm code allows flexibility to alter the value surface albedo
55 in time and wavelength (Campanelli et al., 2015).”

56

57 RC: I still suggest using greater characters for Figure 2, 3, 4. It has been difficult reading the
58 statistics values.

59 AR: Figure 2, 3, and 4 are reproduced with bigger size characters and numbers.

60

61

62 Response to Referee # 2

63

64 RC: Referee's comment

65 [AR: Author's response](#)

66

67 RC: The present study deals with the assessment of SSA derived by the OMI sensor against the
68 corresponding retrievals obtained from ground SKYNET stations. Most of the issues addressed
69 here have been already discussed in Jethva et al. (2014, JGR) and therefore the contribution of
70 the current work is relatively small. An "innovative" aspect is the availability of coincident OMI-
71 SKYNET UV wavelengths (in contrast to AERONET) thus allowing the direct intercomparison
72 between spaceborne and ground-based measurements. Nevertheless, a significant portion of
73 the ground retrievals is coming from POM01 instruments (longer wavelengths of 400nm)
74 requiring the extrapolation of OMI SSA based on the assumed aerosol model in the retrieval
75 algorithm. Below are listed my comments which should be clarified by the authors prior the
76 publication of the submitted manuscript.

77

78 [AR: While we agree with the reviewer that the present study follows our earlier paper of OMI-
79 AERONET SSA comparison \(Jethva et al., 2014\), the present study is the first-ever attempt to
80 evaluate the OMI SSA retrievals against those of SKYNET. The POM-02 sensors owing to its
81 retrievals in the near-UV region facilitates direct comparison with those of OMI at 388 nm. The
82 POM-01 sensors, on the other hand, do not carry UV wavelength filters, but offer retrievals at
83 400 nm requiring an extrapolation of OMI SSA to only 12-nm window against 52-nm when
84 compared with AERONET at 440 nm. It is reasonably fair to assume that the extrapolation of
85 OMI SSA in a narrow window of only 12-nm should not be a major source of uncertainty in
86 comparing SSA from OMI and SKYNET. An additional analysis comparing OMI SSA with POM01
87 and POM02 dataset separately, which is discussed later in this response, suggests that the
88 resultant OMI-SKYNET statistics do not change significantly regardless of the use of POM01 or
89 POM02 in the evaluation.](#)

90

91 In the revised manuscript, it is stated that,

92

93 ["It is reasonably fair to assume that the extrapolation of OMI SSA in a narrow window of 12-nm,
94 i.e., from 388 to 400 nm, shouldn't be a major source of uncertainty in comparing SSA from
95 OMI and SKYNET."](#)

96

97

98 RC: 1. Lines 225-227: The selection of degrees (variable with latitude) instead of distance has
99 impact on the area which is averaged for the OMI retrievals. How much important is this for the
100 overall results?

101 [AR: We attempted several spatial windows for the OMI averaging, i.e., 0.1°, 0.25°, 0.5°, or even
102 1.0°. However, the statistical results in terms of RSMD and % matchups within 0.03/0.05 and
103 derived conclusion didn't alter much. We choose a spatial window of 0.5° centered at SKYNET
104 station to be consistent with our earlier work of comparing OMI and AERONET SSA.](#)

105

106 RC: 2. Lines 235-237: How much reliable are the aerosol models considered in the OMI retrieval
107 algorithm? This is critical since an inappropriate selection of an aerosol model can lead to
108 unrealistic SSA retrievals and subsequently will have impact on the intercomparison outputs.

109
110 AR: The aerosol size distribution and spectral dependence of AOD assumed for all three
111 standard aerosol types considered in the OMAERUV algorithm are based on the AERONET
112 ground-based inversions reported in Dubovik et al. (2002). The spectral dependence of
113 absorption, often quantified as Absorption Angstrom Exponent, for the carbonaceous smoke
114 aerosols accounts for the presence of organics in biomass burning aerosols and referenced to
115 the in-situ absorption measurements taken during SAFARI-2000 experiment (Kirchstetter et al.,
116 2004; Jethva and Torres, 2011). In the latest OMAERUV product used in the present study, the
117 urban-industrial aerosol model is also revised to adopt the same spectral dependence of
118 absorption that of the smoke model. The expected uncertainty of ± 0.03 in the retrieved-SSA
119 accounts for an error in the selection of aerosol model.

120
121 RC: Line 244: Please provide an explanation about the uncertainty limits (Q_0.03 and Q_0.05).
122 Have they been arbitrarily selected?

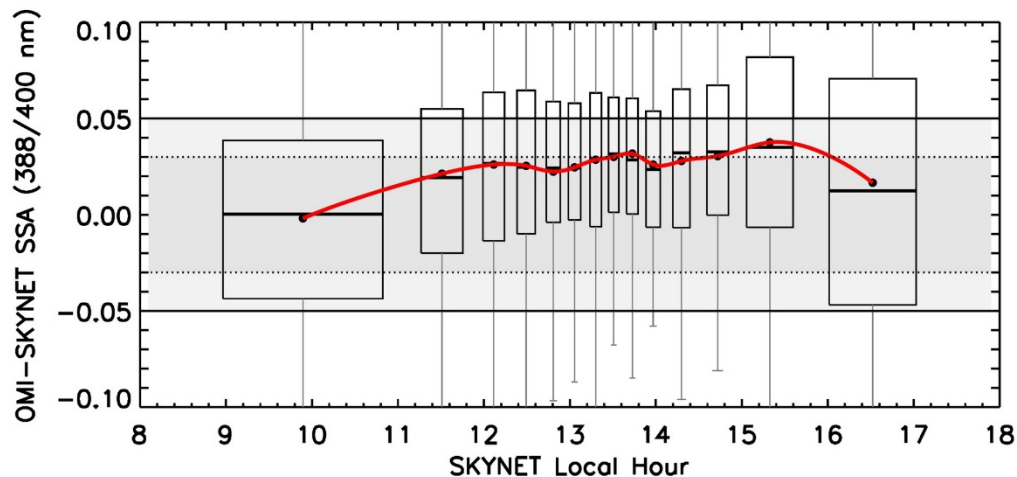
123 AR: The uncertainty limits of OMAERUV SSA retrievals, i.e., ± 0.03 and ± 0.05 were determined
124 based on its comparison with AERONET SSA inversion reported in Torres et al. (2007). Following
125 the early evaluation of OMI aerosol product for a handful of sites, Jethva et al. (2014)
126 conducted a global evaluation of SSA product and also conducted a detailed uncertainty test
127 considering different sources of errors, such as aerosol model, surface albedo, and aerosol layer
128 height. The results of the sensitivity analysis suggested that overall, OMI SSA retrievals are
129 uncertain to within 0.03 to 0.05, however errors could be even larger when algorithmic
130 assumptions are far off from the real atmospheric conditions. This has been clarified in the
131 section 2.1 of the revised paper.

132
133 RC: Section 3.3: Are there any quantified dependencies on the solar zenith angle, station
134 altitude or aerosol layer height?

135 AR: The OMAERUV algorithm does consider the variation in altitude over land in the inversion
136 by interpolating the radiances in terrain pressure in logarithmic space. Therefore, we don't
137 expect significant error in the OMI SSA retrievals due to varying terrain pressure from one
138 station to another. The aerosol layer height (ALH) assumed in each valid retrieval is referenced
139 to the 30-month long CALIOP-OMI $1^\circ \times 1^\circ$ global database [Torres et al., 2013]. Results obtained
140 from a sensitivity study reported in Jethva et al. [2014] suggested that a decrease in the
141 assumed ALH from 3 km to 1.5 km for the dust aerosol type results in a decrease in SSA by 0.02.
142 Although, the climatology dataset of CALIOP-OMI adequately describes the observed mean
143 layer of carbonaceous and desert dust aerosols, variations in the ALH not observed by CALIOP,
144 therefore, will be missed out in the derived climatology and thus can be a source of uncertainty.
145 Assuming that the CALIOP-OMI ALH dataset is accurate to within ± 1 km, the resultant error in
146 SSA retrieval would be $\sim \pm 0.01$.

147
148 The dependence of SSA difference on the local hour of SKYNET measurements are quantified in
149 the Figure shown below. The SKYNET dataset accessed from the data server at Chiba University

150 doesn't contain information on the solar zenith angle. However, the local time of
 151 measurements reported in data file for each station can serve a proxy for the solar zenith angle.
 152 The OMI-SKYNET matchups exhibit a systematic dependency, where the differences between
 153 the two datasets become relatively minimal when early morning and late afternoon inversions
 154 of SKYNET associated with higher solar zenith angle are collocated with OMI retrievals around
 155 1:30 PM local time overpass. Owing to a longer atmospheric optical path at higher solar zenith
 156 angle, thereby better aerosol signal, the ground-based aerosol inversions, such as from
 157 AERONET and SKY
 158 NET, are expected to be more reliable for sky measurements carried out during early
 159 morning/late afternoon.
 160



161
 162 *The difference in SSA between OMI and SKYNET is related to the local measurement hour of*
 163 *SKYNET.*

164
 165 The results obtained in this analysis are added to the discussion in the revised manuscript.
 166

167
 168 RC: Lines 389-395: Unfortunately, the number of OMI-SKYNET pairs is limited in order to extract
 169 robust results. Moreover, how much can affect the irregularity of dust particles' shape? (see
 170 Gasteiger et al. (2011); <https://www.tandfonline.com/doi/pdf/10.1111/j.1600-0889.2011.00559.x?needAccess=true>
 171

172
 173 AR: The collocation procedure yields fewer OMI-SKYNET matchups for the dust aerosol type
 174 identified with the OMAERUV algorithm. The sensitivity study followed by an actual inversion of
 175 OMI data presented in *Torres et al. (2018)* demonstrates that the change in dust particle shape
 176 from spherical to spheroidal distribution improved the AOD retrievals significantly and brought
 177 the equivalency between the retrievals over left and right sides of the OMI swath for the dust
 178 belt region of tropical Atlantic. The associated changes in SSA retrievals were noted within
 179 ± 0.01 and -0.02 for the scattering angle up to 100° - 150° and $>160^\circ$, respectively. The
 180 OMAERUV version 1.8.9.1 data product used in the present study adopts spheroidal dust model

181 based on the work of *Dubovik et al. (2006)* and *Torres et al. (2018)*. We have elaborated the
182 discussion on this aspect of the OMI aerosol retrievals in the uncertainty section 4.2.

183

184 RC: Lines 431-436: These two sentences are confusing. Since the absorption signal increases
185 with height why the SSA values are also increase (i.e., less absorbing particles)?

186 AR: We realized that the information presented here is miscommunicated. The corrected
187 sentence should be,

188

189 “This is because an increase (decrease) in the assumed aerosol layer height from the actual one
190 enhances (reduces) absorption in the radiance look-up table (not in the actual TOA
191 measurements), which the OMAERUV algorithm compensates by retrieving lower (higher) AOD
192 and higher (lower) SSA to match with the observations.”

193

194

195 RC: Lines 442-444: How exactly MODIS is used in the OMI near-UV surface albedo database?

196 AR: The new OMI-based near-UV surface albedo database was essentially derived based on the
197 minimum reflectivity approach. The 7-year record of OMI observation of Lambertian Equivalent
198 Reflectivity or LER at 388 was used to find its minimum value corresponding to UVAI<0.5 for
199 each grid (0.25°x0.25°) and for each month. The 354-nm LER values are anchored to the
200 corresponding minimum LER at 388 nm. During the persistent cloudy period for grids identified
201 with higher LER values and abrupt temporal variations, the information on monthly variations
202 of high-res MODIS surface albedo dataset aligned with the corresponding temporal record of
203 OMI minimum LER was used to estimate LER in the near-UV.

204

205 RC: Section 4.2: In the discussion of this section there are not plots quantifying the OMI-SKYNET
206 declinations with respect to cloud contamination, aerosol layer height and the prescribed
207 surface albedo.

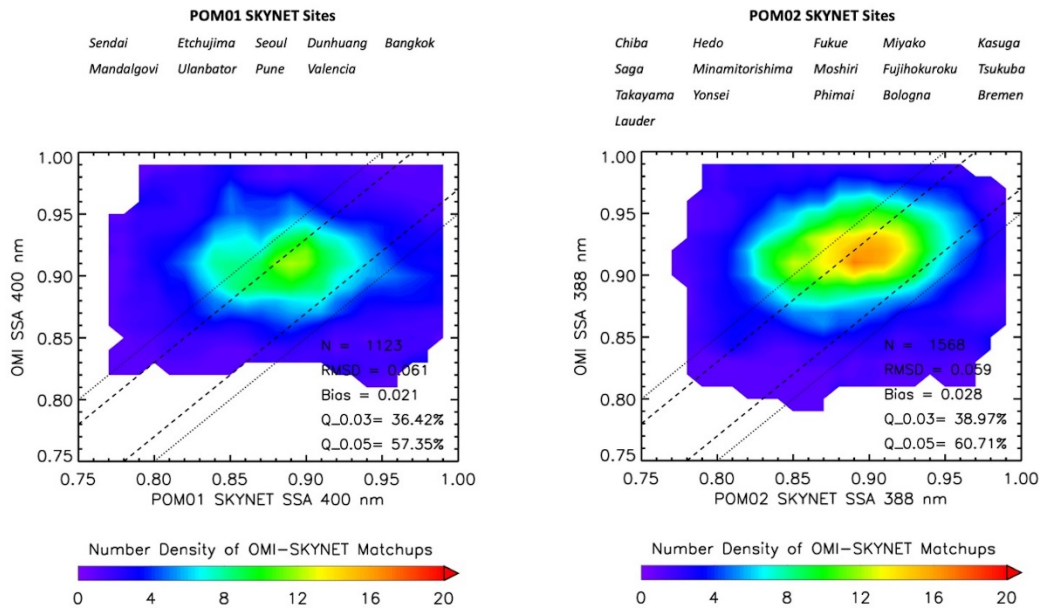
208 AR: The dependence of the SSA difference between OMI and SKYNET as a function of difference
209 in the surface albedo assumption are already shown in Figure 6 and discussed in the section 4.2
210 in the manuscript. Regarding the cloud contamination, we use the ‘best’ quality retrievals from
211 both sensors OMI (final algorithm quality flag=0) and SKYNET (cloud flag=0) in this study largely
212 eliminating the chances of significant cloud interference in both kinds of measurements. Given
213 the larger footprint size of OMI (13x24 km²), however, the possibility of sub-pixel cloud
214 contamination cannot be ruled out completely. On the other hand, a good level of agreement
215 between the two retrievals at higher aerosol loading, and when the differences in the surface
216 albedo reduces to minimum, are indicative of a consistency under favorable conditions. The
217 explanation on the aerosol layer height assumption is explained in response to one the previous
218 comments.

219

220 RC: Figures 4-5-6: Which is the difference on the obtained overall results when POM01 and
221 POM02 SKYNET retrievals are grouped separately?

222 AR: Figure displayed below shows the number density plot comparing SSA between SKYNET and
223 OMI for POM01 and POM02 sensors separately. Overall, we don’t see a major difference in the
224 derived statistics between the two sets of comparison, except that the number of matchups

225 obtained with POM02 sensor is 39% more than those with POM01 sensors and POM02 dataset
 226 offers marginally better comparison (except bias, which is higher with POM02) with OMI SSA
 227 retrievals. This analysis indicates that the interpolation of OMI SSA from 388 nm to 400 nm for
 228 its comparison with POM01 data isn't a significant source of discrepancy between the two SSA
 229 datasets. The revised manuscript includes the new analysis and related discussion.
 230



231
 232 **Figure** Number density plots of SSA comparison between OMI and SKYNET matchups derived
 233 separately using POM-01 (left) and POM-02 (right) sensors. The resultant statistics of the
 234 comparison are depicted in the lower-right in each plot.

235

236 **A Comparative Evaluation of Aura-OMI and**
237 **SKYNET Near-UV Single-scattering Albedo**
238 **Products**
239

240
241 Hiren Jethva^{1,2*}, Omar Torres²

242
243 ¹Universities Space Research Association, Columbia, MD 21044 USA

244 ²NASA Goddard Space Flight Center, Greenbelt, MD 20771 USA
245

246
247
248
249
250 **Mailing Address:**

251 Room#A422, Building#33,

252 Laboratory of Atmospheric Chemistry & Dynamics

253 Earth Science Division

254 NASA Goddard Space Flight Center,

255 Greenbelt, MD 20771, USA
256

257 *** Corresponding Author: Dr. Hiren Jethva**

258 **E-mail: hiren.t.jethva@nasa.gov**

259 **ABSTRACT**

260 The aerosol single-scattering albedo (SSA) retrieved by the near-UV algorithm applied to the
261 Aura/Ozone Monitoring Instrument (OMI) measurements (OMAERUV) is compared with an
262 independent inversion product derived from the sky radiometer network SKYNET—a ground-
263 based radiation observation network span over Asia and Europe. The present work continues
264 our efforts to evaluate the consistency between the retrieved SSA from satellite and ground
265 sensors. The automated spectral measurements of direct downwelling solar flux and sky
266 radiances made by SKYNET Sun-sky radiometer are used as input to an inversion algorithm that
267 derives spectral aerosol optical depth (AOD) and single-scattering albedo (SSA) in the near-UV
268 to near-IR spectral range. The availability of SKYNET SSA measurements in the ultraviolet region
269 of the spectrum allows, for the first time, a direct comparison with OMI SSA retrievals
270 eliminating the need of extrapolating the satellite retrievals to the visible wavelengths as the
271 case in the evaluation against the Aerosol Robotic Network (AERONET). An analysis of the
272 collocated retrievals from over 25 SKYNET sites reveals that about 61% (84%) of OMI-SKYNET
273 matchups agree within the absolute difference of ± 0.03 (± 0.05) for carbonaceous aerosols, 50%
274 (72%) for dust aerosols, 45% (75%) for urban-industrial aerosol types. Regionally, the
275 agreement between the two inversion products was robust over several sites in Japan
276 influenced by carbonaceous and urban-industrial aerosols, at the biomass burning site *Phimai*
277 in Thailand, and polluted urban site in *New Delhi*, India. The collocated dataset yields fewer
278 matchups identified as dust aerosols mostly over the site *Dunhuang* with more than half of the
279 matchup points confined to within ± 0.03 limits. Combinedly, the OMI-SKYNET retrievals agree
280 mostly within ± 0.03 for the AOD (388 or 400 nm) larger than 0.5 and UV Aerosol Index larger
281 than 0.2. The remaining uncertainties in both inversion products can be attributed to specific
282 assumptions made in the retrieval algorithms, i.e., the uncertain calibration constant,
283 assumption of spectral surface albedo and particle shape, and sub-pixel cloud contamination.
284 The assumption of fixed and spectrally neutral surface albedo (0.1) in the SKYNET inversion
285 appears to be unrealistic, leading to ~~a large underestimation of retrieved~~ SSA, especially
286 ~~under~~ for lower aerosol load conditions. At ~~higher~~ large AOD values for carbonaceous and dust

287 aerosols, however, retrieved SSA values by the two independent inversion methods are
288 generally consistent in spite of the differences in retrieval approaches.

289 1 INTRODUCTION

290 Satellite-based remote sensing of aerosols has become an essential tool to detect, quantify, and
291 routinely monitor the aerosol optical and size properties over the globe. An accurate
292 representation of aerosols in the climate models is an essential requirement for reducing the
293 uncertainty in aerosol-related impact on the Earth's radiation balance (direct and semi-direct
294 effects) and cloud microphysics (indirect effect) (*IPCC*, 2013). The fundamental aerosol
295 parameters determining the strength and sign of the radiative forcing are the aerosol optical
296 depth (AOD) and single-scattering albedo (SSA) in addition to the reflective properties of the
297 underlying surface. While the columnar AOD represents the total extinction (scattering and
298 absorption) resulting from the interactions with solar radiation, SSA describes the relative
299 strength of scattering to the total extinction. Together, both AOD and SSA determine the
300 magnitude and sign of the aerosol radiative forcing [at the top-of-atmosphere](#). For example, a
301 decrease in SSA from 0.9 to 0.8 can often change the sign of radiative forcing from negative
302 (cooling) to positive (warming) that also depends on the albedo of the underlying surface and
303 the altitude of the aerosols (*Hansen et al.*, 1997). Thus, an accurate estimate of both quantities
304 is a prime requirement for reliable estimates of the net effect of atmospheric aerosols
305 produced with the anthropogenic as well as natural activities.

306

307 Launched in July 2004, the Ozone Monitoring Instrument (OMI) onboard NASA's Aura satellite
308 has now produced more than a decade long global record of observations of reflected radiation
309 from Earth in the 270–500 nm wavelength range of the spectrum on a daily basis. OMI scans
310 the entire Earth in 14 to 15 orbits with its cross-track swath of ~2600 km at ground level at a
311 nadir ground pixel spatial resolution of 13×24 km². Satellite observations of the top-of-
312 atmosphere reflected light at 354 and 388 nm wavelengths made by OMI are used to derive the
313 UV aerosol index (UVAI) as well as the AOD and SSA using a near-UV algorithm (OMAERUV) that
314 takes advantage of the well-known sensitivity to the aerosol absorption in the UV spectral
315 region (*Torres et al.*, 1998). While a general description of the OMI/OMAERUV algorithm is
316 presented in *Torres et al.* (2007), the recent algorithmic upgrades are documented in *Torres et*

317 *al.* (2013, 2018). The most important changes applied in the latest OMAERUV algorithm
318 upgrade includes: 1) use of new carbonaceous aerosol models that account for the presence of
319 organics in the carbonaceous aerosols by assuming wavelength-dependent imaginary part of
320 the refractive index (*Jethva and Torres, 2011*), 2) an implementation of robust scheme to
321 identify aerosol type (smoke, dust, urban/industrial) that combinedly uses the information on
322 carbon monoxide (CO) observations from the Atmospheric Infrared Sounder (AIRS) and UVAI
323 from OMI (*Torres et al., 2013*), 3) use of the aerosol height climatology dataset derived from
324 the Cloud-Aerosol Lidar with Orthogonal Polarization (CALIOP) lidar-based measurements of
325 the vertical profiles of aerosol for the carbonaceous and dust aerosols (*Torres et al., 2013*), and
326 4) better treatment of dust particles assuming realistic spheroidal shape distribution (*Torres et*
327 *al., 2018*). Additionally, the upgraded OMAERUV algorithm has adopted a new method to
328 calculate UVAI, which now accounts for the angular scattering effects of clouds and significantly
329 reduces a scan angle related asymmetry in UVAI ~~in over~~ cloudy scenes (*Torres et al., 2018*).

330

331 The present work continues our efforts to evaluate the consistency between ground-based SSA
332 measurements and satellite retrievals from near UV observations. On the first attempt to
333 intercompare space-based and surface near UV SSA measurements, Earth Probe TOMS
334 retrievals were compared to AERONET observations acquired during the SAFARI 2000 field
335 campaign (*Torres et al., 2005*). The OMAERUV near-UV aerosol product of AOD and SSA has
336 been continually assessed and validated against the ground-based measurements acquired
337 from the globally distributed Aerosol Robotic Network-AERONET (*Torres et al., 2007; Ahn et al.,*
338 *2008; Jethva and Torres, 2011; Ahn et al., 2014; Jethva et al., 2014*). While the OMAERUV AOD
339 product was directly validated against the AERONET measurements made in the near-UV (340-
340 380 nm), as carried out in *Ahn et al. (2014)*, the SSA retrievals have been evaluated by
341 comparing with an independent ground inversion product of AERONET by *Jethva et al. (2014)*.
342 The latter analysis required OMI retrievals of SSA to be extrapolated to the shortest visible
343 wavelength of 440 nm of AERONET inversion product to make the comparison possible. Such
344 adjustment in the wavelength of retrievals can introduce uncertainty in the comparison arising

345 from inaccuracy of the spectral dependence of absorption assumed in the wavelength
346 conversion.

347

348 A direct comparison of the column-integrated SSA at 388 nm retrieved from OMI requires
349 equivalent ground-based columnar retrievals in the near-UV region. The international network
350 of scanning sun-sky radiometers (SKYNET) fulfills this requirement as it performs the direct Sun
351 and sky measurements in the near-UV (340-380 nm) as well as visible/near-IR (400-1020 nm)
352 regions of the spectrum, and derives spectral AOD and SSA at these wavelengths. Taking
353 advantage of the availability of ground-based SSA inversions in the near-UV from SKYNET, we
354 inter-compare the OMI and SKYNET SSA products at several SKYNET sites in Asia and Europe.
355 Since both retrieval approaches are based on inversion algorithms that rely on assumptions, the
356 resulting level of agreement can only be interpreted as a measure of consistency (or lack
357 thereof) in the measurement of the same physical parameter by fundamentally different
358 remote sensing approaches.

359

360 The paper is organized as follows: [Section 2](#) describes the satellite and ground-based data sets
361 assessed in this analysis along with the collocation methodology; the results of OMI-SKYNET
362 SSA comparison over individual sites, combinedly for each aerosol type, and diagnosis of
363 differences between them are presented in section 3; the possible sources of uncertainty in
364 both inversion products are discussed in section 4; the paper is summarized and concluded in
365 section 5.

366

367 **2 DATASETS**

368 **2.1 THE OMI-OMAERUV AEROSOL PRODUCT**

369 The entire record of OMI observations (October 2004 to present) has been reprocessed
370 recently with the refined OMAERUV algorithm (PGEVersion V1.8.9.1) to derive a comprehensive

371 aerosol product that includes the retrievals of UV Aerosol Index (UVAI), AOD, SSA, and AOD
372 (388 nm) at a pixel resolution of 13 x 24 km² at nadir viewing geometry. The retrieved
373 parameters are also reported at 354 nm and 500 nm wavelengths following the spectral
374 dependence of aerosols assumed in the chosen model. The data set is available in the HDF-
375 EOS5 format and can be obtained at no cost from NASA Goddard Earth Sciences (GES)-Data and
376 Information Services Center (DISC) server at <http://daac.gsfc.nasa.gov/>. The recent upgrade has
377 been documented in detail in the work of *Jethva and Torres (2011)*, *Torres et al. (2013, 2018)*
378 and *Ahn et al. (2014)*. Here, we use the OMAERUV Level 2 Collection 003 (V1.8.9.1) aerosol
379 product processed in July 2017. The expected uncertainty limits in the OMAERUV SSA retrievals
380 are determined to be ±0.03 and ±0.05, based on its comparison with AERONET SSA inversion
381 and sensitivity analysis carried out during the development of the OMAERUV algorithm (Torres
382 et al., 2007). Following an early evaluation of OMI aerosol product for a handful of sites, Jethva
383 et al. (2014) conducted a global evaluation of SSA product and also carried out a detailed
384 uncertainty test considering different sources of errors, such as aerosol model, surface albedo,
385 and aerosol layer height. The results of the sensitivity analysis further confirmed the
386 uncertainty budget estimated earlier during the early development of the OMAERUV algorithm.
387 However, note that the errors could attain larger magnitudes when algorithmic assumptions
388 are far off from the real atmospheric conditions.

389
390 Post-2007, the OMI observations have been affected by a possible external obstruction that
391 perturbs both the measured solar flux and Earth radiance. This obstruction affecting the quality
392 of radiance at all wavelengths for a particular viewing direction is referred to as “row anomaly”
393 (RA) since the viewing geometry is associated with the row numbers on the charge-coupled
394 device detectors. The RA issue was detected first time in mid-2007 with a couple of rows which
395 during the later period of operation expanded to other rows in 2008 and later. At present,
396 about half of the total 60 rows across the track are identified and flagged as row anomaly
397 affected positions for which no physical retrievals are performed (*Schenkeveld et al., 2017*). The
398 details about this issue can be found at
399 <http://www.knmi.nl/omi/research/product/rowanomaly-background.php>. The RA has

400 significantly affected the sampling during post-2008 OMI measurements, where row anomaly
401 flags blanket about half of the OMI swath. ~~about half of the OMI swath is blanketed by row~~
402 ~~anomaly flags~~. As a result, the availability of the number of retrievals over a particular station
403 is reduced starting in 2009 compared to earlier OMI measurements. Therefore, Consequently,
404 the OMI-SKYNET matchups are also expected to be lower during the row anomaly affected
405 period. The OMAERUV algorithm assigns quality flags to each pixel which carries information on
406 the quality of the retrieval depending upon the observed condition. We used aerosol retrievals
407 free of RA and flagged as quality flag '0', which are considered best in accuracy due to higher
408 confidence in detecting aerosols in a scene with minimal or no cloud contamination.

409 2.2 THE SKYNET AEROSOL INVERSION PRODUCT

410 The SKYNET is an international network of scanning sun-sky radiometers (manufactured by
411 *Prede Co. Ltd.*, Japan) performing routine and long-term measurements of direct and diffuse
412 solar radiations at several wavelengths spanning UV (340 and 380 nm), visible (400, 500, 675
413 nm), near-IR region (875, 1020 nm), and in shortwave-IR (1627 nm and 2200 nm) of the
414 spectrum. The automated measurements of direct and diffuse solar radiations are used to
415 measure spectral AODs and retrieve SSAs and other aerosol optical-microphysical properties
416 (volume size distribution, refractive index, phase function, and asymmetry parameter) at the
417 same standard wavelengths of AOD following an inversion algorithm packaged in the
418 *SKYRAD.pack* software (*Nakajima et al.*, 1996; *Hashimoto et al.*, 2012). Cloudy observations are
419 screened using the Cloud Screening Sky Radiometer code (*Khatri and Takamura*, 2009).

420
421 The SKYNET radiometers come in two flavors, model POM-01 and model POM-02. The POM-01
422 instrument carries a total of five wavelength filters covering visible to near-IR (400-1020 nm),
423 whereas POM-02 instrument has two additional filters in the UV region (340 and 380 nm) along
424 with the other filters in the visible to shortwave-IR (including 1627 nm and 2200 nm) part of the
425 spectrum. The calibration of each SKYNET radiometer is performed on-site on a monthly basis
426 using the improved Langley method (*Nakajima et al.*, 1996; *Campanelli et al.*, 2004, 2007).
427 Occasionally, the inter-calibration of radiometers is carried out against the master instrument

428 well-calibrated using the Langley method at a high mountain site, e.g., Mauna Loa. The SKYNET
429 radiometers are also inter-compared with AERONET Cimel Sunphotometers and precision filter
430 radiometers at three observation sites, i.e., *Chiba University*, ~~and~~ *Valencia (Estelles et al., 2016)*,
431 ~~and~~ *Rome (Campanelli et al., 2018)*.

432
433 Studies in the past have compared AODs (*Estellés et al., 2012a*) and SSAs (*Estellés et al., 2012b*)
434 measured/retrieved from SKYNET and AERONET and shown that AODs are well-correlated and
435 in good agreement, but the SKYNET SSAs are found to be higher than those of AERONET (*Che et*
436 *al., 2008; Hashimoto et al., 2012*). *Khatri et al. (2016)* further pinpoints the factors, such as
437 quality of input data attributed to different calibration and observation protocol, different
438 quality assurance criteria, the calibration constant for sky radiances, differences in measured
439 AOD, and surface albedo, responsible for the inconsistent aerosol SSA between AERONET and
440 SKYNET using observations from the four representative sites, i.e., Chiba (Japan), Pune (India),
441 Valencia (Spain), and Seoul (South Korea). More discussion on the sources of uncertainties is
442 presented in section 4.

443
444 In this study, we include the SKYNET data acquired over a total of 25 sites distributed mostly
445 across Asia and a few in Europe. The dataset is freely ~~accessible~~accessible from the data ~~holding~~
446 portal of the Center for Environmental Remote Sensing (CERes), Chiba University, Japan
447 (<http://atmos3.cr.chiba-u.jp/skyenet/data.html>). Figure 1 shows the geographic distribution of
448 selected sites, whereas Table 1 lists the geo-coordinates of these sites with the associated
449 sensor type (POM-01 or POM-02) and data periods. The SKYNET aerosol product is derived
450 using two different Skyrad packs: version 4.2 and version 5, the differences of which are
451 explained in *Hashimoto et al. (2012)*. In this study, we use the SKYNET Level 2 product retrieved
452 using version 5 of Skyrad pack. SKYNET retrievals assigned with cloud flag '0' are included in the
453 analysis, ~~since~~ since these measurements are ~~believed~~ to be free of cloud contamination considered
454 as higher quality retrievals. A careful examination of the SKYNET inversion dataset revealed
455 some irregularities in the measurements for many sites, such as irregular patterns in the shape
456 of spectral SSAs, identical values of SSA at near-UV and visible wavelengths, and much larger

457 standard deviation (>0.1) in SSA within a few hours. These spurious measurements were
458 excluded from the present analysis.

459 **2.3 THE COLLOCATION OF OMI AND SKYNET MEASUREMENTS**

460 OMI retrievals correspond to a spatial scale of $13 \times 24 \text{ km}^2$ at nadir representing the
461 atmospheric conditions over an area. Unlike the direct measurements of the spectral AOD,
462 which correspond to columnar point measurements, the retrievals made by SKYNET use the sky
463 radiances measured at several discrete angles azimuthally, therefore representing the sky
464 condition observed over a station which is associated with approximately 5 km radius
465 surrounding the Sun photometer site. SKYNET retrieves aerosol optical-microphysical
466 properties, including spectral SSA, under all cloud-free conditions and at all aerosol loadings. It
467 is expected that the inversion of retrieved parameters from sky radiances offers better accuracy
468 at larger solar zenith angles owing to the longer optical path and better aerosol absorption
469 signal (*Dubovik et al., 2000*). These conditions are best satisfied with the measurements made
470 during the early morning and late afternoon hours. On the other hand, Aura/OMI overpasses a
471 station during the afternoon hours with the local equator-crossing time 1:30 P.M. In order to
472 collocate both types of measurements, therefore we select a time window of $\pm 3 \text{ h}$ around OMI
473 overpass time in order to get sufficient high-quality SKYNET retrievals particularly from early
474 morning/late afternoon measurements. The OMI retrievals of SSA were spatially averaged in a
475 grid area of 0.5° by 0.5° centered at the SKYNET site. Though the spatial averaging area for the
476 OMI retrieval is about 50 km^2 , due to its larger footprint, the actual area intercepted by OMI
477 pixels around SKYNET site is likely to be larger.

478

479 OMI performs retrieval at 354 nm and 388 nm wavelengths, whereas the SKYNET POM-02
480 instrument reports SSA at nearby wavelengths of 340, 380, and 400 nm. To compare both SSA
481 products at the same wavelength, SKYNET SSA was linearly interpolated at 388 nm, to match
482 with the wavelength of OMI retrieval, using the measurements at the two nearest wavelengths,
483 i.e., 380 nm and 400 nm. The SKYNET POM-01 instruments don't carry UV wavelength filters,
484 but report the retrievals at the shortest wavelength 400 nm and other visible/near-IR

485 wavelengths. In this case, the OMI retrievals are extrapolated from 388 nm to 400 nm, to match
486 with the wavelength of SKYNET inversion, following the spectral dependence of SSA associated
487 with the chosen aerosol model in the OMI algorithm. It is reasonably fair to assume that the
488 extrapolation of OMI SSA in a narrow window of 12-nm, i.e., from 388 to 400 nm, should not be
489 a major source of uncertainty in comparing SSA from OMI and SKYNET.

490 **3 RESULTS**

491 **3.1 OMI-SKYNET COMPARISON OVER INDIVIDUAL STATIONS**

492 Figure 2 displays the OMAERUV versus SKYNET SSA scatterplots for selected sites in Japan. The
493 comparison was made at 388 nm or 400 nm depending upon the availability of the SKYNET
494 inversion at those wavelengths, i.e., POM-01 or POM-02 sensors. Legends with different colors
495 represent the aerosol type selected by the OMAERUV algorithm for the co-located matchups
496 (N). RMSD is the root-mean-square difference between the two retrievals; Q_0.03 and Q_0.05
497 are the percent of total matchups (N) that fall within the absolute difference of 0.03 and 0.05,
498 respectively; horizontal and vertical lines for each matchup are the standard deviation of
499 temporally and spatially averaged SKYNET and OMI SSAs. The comparison includes OMI-SKYNET
500 matchups with AOD>0.3 (388 or 400 nm) in both measurements simultaneously. The
501 scatterplots reveal a good level of agreement for matchups identified with
502 carbonaceous/smoke aerosols over *Chiba University, Cape Hedo, Fukue, Saga, and Etchujima*
503 with the majority of points confined within the absolute difference of 0.03. The OMI-SKYNET
504 combined dataset is dominated with matchup points identified as the urban/industrial
505 aerosols by the OMAERUV algorithm for which the measured UVAI falls below 0.5 representing
506 lower aerosol loading in the boundary layer with weakly absorbing properties. Under such
507 observed conditions, the uncertainties in both kinds of measurements are prone to be larger
508 due to lower absorption signal relative to the instrumental noise and errors in algorithmic
509 assumptions, such as surface albedo, that could further amplify the overall uncertainty in the
510 retrievals. Despite these inherent uncertainties, an agreement within the difference of ± 0.03

511 for about or more than half of the collocated retrievals is encouraging. A more detailed
512 description of the different sources of uncertainty is presented in the next section.

513

514 Figure 3 shows the scatterplots of OMI-SKYNET SSA for remaining sites located in South Korea,
515 China, Thailand, India, and Italy. For the site *Seoul* in South Korea, OMI tends to overestimate
516 SSA for a number of matchups assigned with the urban/industrial aerosol type and for a few
517 with the carbonaceous/smoke aerosol type such that about 42% of total matchups are falling
518 within the difference of 0.03. For the *Dunhuang* site located in the desert area of China, a
519 majority of collocated data points were identified as dust aerosol type providing an overall
520 better agreement with 50% and 68% matchups bounded within ± 0.03 and ± 0.05 differences,
521 respectively. The *Phimai* site in Thailand is known to be influenced by the springtime biomass
522 burning activities, where OMI and SKYNET SSAs are found to agree relatively best among all 25
523 sites providing 71% and 91% of the matchups restricted within ± 0.03 and ± 0.05 limits,
524 respectively. The agreement between the two sensors was robust for the carbonaceous/smoke
525 aerosol type followed by the urban/industrial aerosols. Over the megacity of New Delhi in the
526 Indo-Gangetic Plain in India, which is seasonally influenced by the smoke and desert dust
527 aerosols in addition to the local source of urban pollution, the OMI-SKYNET matchups are found
528 to agree within ± 0.03 and ± 0.05 for 52% and 83% of the evaluated data points respectively.
529 Over the *Pune* station located near the western boundary of India and the *Bologna* site in Italy,
530 OMI retrieves higher SSA compared to that of SKYNET yielding 39% and 64%, and 25% and 50%
531 matchups, respectively, within the two uncertainty limits. Table 1 lists the statistical measures
532 of the OMI-SKYNET SSA comparison for all 25 sites.

533 **3.2 COMPOSITES FOR EACH AEROSOL TYPE**

534 Figure 4 displays the composite scatterplots of OMI versus SKYNET SSA derived by segregating
535 the matchup points for each aerosol type from all 25 sites. The intention here is to evaluate the
536 consistency between the two retrieval methods for each aerosol type separately and
537 understand their relative differences. When identified as the carbonaceous/smoke aerosol type,
538 the OMI-SKYNET matchups reveal relatively best comparison among the three major aerosol

539 types with 61% and 84% data points falling within the absolute difference of 0.03 and 0.05,
540 respectively, and providing the lowest (0.035) root-mean-square-difference between the two
541 retrievals. The collocation procedure yields the lowest number of matchups (N=32) for desert
542 dust aerosol type obtained mostly over the site of *Dunhuang* in China, resulting 50% and 72% of
543 data points within the stated uncertainty limits. Among the three aerosol types, the collocated
544 points assigned with the urban/industrial aerosol type (Figure 4 bottom-left) yield the
545 maximum number of matchups (N=739) with the relatively weakest agreement (RMSD=0.052),
546 where OMI tends to overestimate SSA for a significant number of instances resulting about 45%
547 and 67% data points falling within the two limits of expected uncertainties. When more than
548 one prescribed aerosol types are selected for OMI pixels around the SKYNET stations, the
549 matchups between the two sensors resulted in 59% and 77% retrievals within the uncertainty
550 limits with an RMSD of 0.041—a comparison slightly poorer than ‘smoke-only’ case, but better
551 than ‘dust-only’ and ‘urban/industrial-only’ retrieval cases. Combined, all three distinct aerosol
552 types simultaneously yield the total number of matchups (N=1223) with an RMSD of 0.047
553 between OMI and SKYNET resulting 51% and 72% collocated data points falling within the
554 absolute difference of 0.03 and 0.05 difference, respectively. When the restriction of $AOD > 0.3$
555 is removed from the collocation procedure, allowing all matchups regardless of their respective
556 AOD values, the total number of collocated data points was increased to more than twice
557 (N=2691) albeit with a relatively weaker agreement yielding an RMSD of 0.06 and percent data
558 points within the uncertainty limits reducing to 38% and 59%, respectively.

559

560 **3.3 COMPOSITES FOR VARYING AEROSOL LOADING AND POM-01 VERSUS POM-02**

561 Figure 5 shows the number density plots comparing OMI-SKYNET SSA matchups obtained from
562 all sites combined and for the three aerosol loading conditions. The best set of comparison is
563 achieved under the most restrictive scenario when corresponding OMI-retrieved AOD and UVAI
564 are constrained to >0.3 and >0.5 , respectively, albeit with a significantly reduced number of
565 matchups compared to the other two cases with lesser (middle) or no (left) restrictions. The
566 improved comparison reflected in statistical parameters is a result of avoiding retrievals with

567 lower aerosol loading when both kinds of measurements might be subjected to larger
568 uncertainties due to algorithmic assumptions.

569
570 Figure 6 shows the number density plot comparing SSA between SKYNET and OMI for POM-01
571 and POM-02 sensors separately. Overall, no major difference noticed in the derived statistics
572 between the two sets of comparison except that the number of matchups obtained with
573 POM02 sensor is 39% more than those with POM01 sensors, and POM02 dataset offers
574 marginally better comparison (except bias, which is higher with POM02) with OMI SSA
575 retrievals. This analysis indicates that the interpolation of OMI SSA from 388 nm to 400 nm for
576 its comparison with POM01 data isn't a significant source of discrepancy between the two SSA
577 datasets.

579 **3.33.4 DIAGNOSIS OF OMAERUV VERSUS SKYNET SSA**

580 The SKYNET algorithm inverts the spectral sky radiances in conjunction with the direct AOD
581 measurements to retrieve the real and imaginary parts of the refractive index and particle size
582 distribution of cloud-free observations under all aerosol loading conditions. These inversion
583 products are believed to be more stable and accurate at ~~higher~~**larger** aerosol loadings and solar
584 zenith angles due to stronger aerosol absorption signal and longer optical path (*Dubovik et al.,*
585 2000). Similarly, a sensitivity analysis of the two-channel OMAERUV retrievals suggests that the
586 retrieved AOD and SSA are susceptible to the small change in surface albedo at lower aerosol
587 loading (*Jethva et al., 2014*). For instance, an absolute difference of 0.01 in the surface albedo
588 leads to a change in AOD approximately by 0.1 and SSA by ~0.02.

589
590 Figure ~~57~~ (top) shows the absolute difference in collocated SSA between OMI and SKYNET as a
591 function of concurrent SKYNET direct AOD (388 or 400 nm) measurements for all aerosol types.
592 All OMI-SKYNET matchup data obtained from a total of 25 sites under all AOD conditions are
593 included here. The data are shown in the box and whisker format, where the horizontal lines

594 represent the median value of each [data](#) bin of sample size 150, filled circle the mean value,
595 and shaded vertical bars cover the 25 and 75 percentiles of the population in each [data](#) bin.
596 While for most bins the mean and median values of SSA difference were restricted to within
597 ± 0.03 , OMI tends to overestimate SSA relative to that of SKYNET at lower AODs giving larger
598 differences and spread in the data population. Similar patterns were observed when the
599 difference in SSA was related to the OMI-retrieved AOD (Figure [75](#) middle). In both cases, the
600 differences in SSA minimize at larger AOD values (>0.5) suggesting a convergence in both
601 retrievals. Figure [75](#) (bottom) shows a similar plot of SSA difference against the concurrent OMI
602 UVAI. Notably, the differences in SSA exhibit even a stronger relationship to UVAI than that in
603 the AOD case (top and middle). For UVAI lesser than zero, the differences in the retrieval are
604 found to be beyond the expected uncertainty in both inversions, at least in the mean sense. For
605 the lower range of UVAI, OMI algorithm mostly employs the urban/industrial model for the
606 retrieval where all aerosols are assumed to be confined within the boundary layer (<2 km) with
607 a vertical profile that follows an exponential distribution. On the other hand, the mean and
608 median values of the SSA difference for UVAI larger than 0.2 for all bins fall within the 0.03
609 uncertainty range. The SSA differences approach to near-zero with a reduced spread at larger
610 magnitudes. Notably, both inversions are found to be in closer agreement for UVAI
611 measurements >0.3 .

612

613

614 4 SOURCES OF UNCERTAINTY

615 4.1 UNCERTAINTIES IN THE GROUND-BASED SKYNET INVERSION PRODUCT

616 The [standard](#) SKYNET inversion algorithm assumes a wavelength-independent surface albedo of
617 0.1 at all wavelengths across the UV to visible part of the spectrum. [However, the algorithm](#)
618 [code allows flexibility to alter the value surface albedo in time and wavelength \(Campanelli et](#)
619 [al., 2015\).](#) The diffuse light reflected from the ground plays a second-order role in the measured
620 sky radiances in most situations, however, has a potential to affect the SSA inversion, e.g.,

621 overestimated (underestimated) surface albedo can underestimate (overestimate) SSA
622 (*Dubovik et al.*, 2000; *Khatri et al.*, 2012). Using simultaneous inversion data from SKYNET and
623 AERONET for four representative sites, *Khatri et al.* (2016) have shown that the difference in
624 the prescribed surface albedo between SKYNET and AERONET results in a difference of ~ 0.04 in
625 SSA at red (675 nm) and near-IR wavelengths retrieved from the two collocated ground sensors.
626 The difference in SSA can also reach as large as ~ 0.08 when surface albedo differed by 0.3. The
627 assumed surface albedo value of 0.1 at near-UV (340 and 380 nm) and shorter visible
628 wavelength (400 nm) seems to be unrealistic for the vegetated and urban surfaces. The surface
629 albedo database at 354 nm and 388 nm derived from multiyear observations from OMI
630 suggests that the vegetated surfaces and urban centers are characterized with the lower values
631 of surface albedo, i.e., ~ 0.02 - 0.03 and ~ 0.05 , respectively; for desert surfaces, the albedo could
632 be as high as 0.08 - 0.10 . Significant differences in the assumed surface albedo values between
633 OMI and SKYNET at shorter wavelengths could be one of the responsible factors for
634 discrepancies in SSA noted over several sites, particularly at lower aerosol loading when the
635 uncertainty in surface characterization can amplify error in the SSA inversion.

636

637 To further investigate this effect, the difference in SSA between OMI and SKYNET as a function
638 of the simultaneous difference in surface albedo is analyzed and shown in Figure 68 (top). The
639 data are presented in a standard box and whisker plot format. Figure 86 reveals a link between
640 differences in SSA and surface albedo, where increasing differences in SSA (OMI>SKYNET) are
641 associated with significant negative biases in surface albedo between OMI and SKYNET. In other
642 words, large overestimation in SKYNET surface albedo causes underestimation of retrieved SSA,
643 which is consistent with the findings of *Dubovik et al.* (2000) and *Khatri et al.* (2012, 2016),
644 thereby resulting in a substantial positive difference in SSA between OMI and SKYNET. Recently,
645 *Mok et al.* (2018) have shown that the use of AERONET surface albedo dataset at 440 nm in the
646 SKYNET algorithm for the S. Korea region produces SSA values larger by ~ 0.01 at near-UV
647 wavelengths. Notably, differences in SSA tend to be lower when the differences in surface
648 albedo are also minimal, such that the mean and median values of those bins remain within the
649 expected uncertainties of ± 0.03 in both retrievals. This result, along with the previous findings

650 cited above, convincingly points out that the SSA inversion from ground-based sensors,
651 especially at lower aerosol loadings, is likely susceptible to the prescribed surface albedo. The
652 assumption of a fixed value of spectral surface albedo of 0.1 in the SKYNET algorithm appears to
653 be inappropriate calling for a revision using more accurate datasets of spectral reflectance or
654 albedo such as from MODIS and OMI.

655

656 The dependence of SSA difference on the local hour of SKYNET measurements is quantified in
657 the Figure 8 (bottom). The SKYNET dataset accessed from the data server at Chiba University
658 doesn't contain information on the solar zenith angle. However, the local time of
659 measurements reported in the data file for each station can serve a proxy for the solar zenith
660 angle. The OMI-SKYNET matchups exhibit a systematic dependency, where the differences
661 between the two datasets become relatively minimal when early morning and late afternoon
662 inversions of SKYNET associated with higher solar zenith angle are collocated with OMI
663 overpass time around 1:30 PM equator-crossing time. Owing to a longer atmospheric optical
664 path at higher solar zenith angle, thereby better aerosol absorption signal, the ground-based
665 aerosol inversions, such as from AERONET and SKYNET, are expected to be more reliable for sky
666 measurements carried out during early morning/late afternoon.

667

668 SKYNET inversion algorithm (Skyrad.pack Version 4.2 and version 5) assumes aerosols of
669 spherical shape regardless of the actual aerosol type observed in the scene. Following a
670 detailed analysis of the effect of non-sphericity of the particles on the difference between the
671 retrievals carried out assuming spherical and spheroidal size distribution, *Khatri et al.*, (2016)
672 concluded that the assumed shape of particles has a non-significant impact on the retrieved
673 SSA. Their study revealed SSA difference of ± 0.01 for measurements having a maximum
674 scattering angle $< 120^\circ$ and difference of up to ± 0.02 at scattering angle $> 120^\circ$, where the
675 difference in the phase function is significant between spherical and spheroidal size
676 distributions (*Torres et al.*, 2018). The OMI-SKYNET collocation procedure, as shown in Figure 4,
677 yields relatively fewer matchups that are identified as dust aerosol type according to the

678 OMAERUV aerosol type identification scheme. A majority of the collocated data points were
679 derived over the desert site of *Dunhuang* in China showing a reasonable agreement in SSA
680 between OMI and SKYNET for dust aerosols further supporting the findings of *Khatri et al.*
681 (2016) that the SSA retrievals are not significantly impacted by the assumption of the shape of
682 particles, i.e., spherical or spheroidal.

683

684 Apart from the algorithmic assumptions, the calibration constant used for sky radiances
685 measured by SKYNET instruments can be a potential source of errors in the inversion. *Khatri et*
686 *al.* (2016) suggests that the calibration constant for sky radiances determined from the disk
687 scan method using solar disk scan area of $1^\circ \times 1^\circ$ (*Boi et al.*, (1999) may be underestimated
688 resulting in overestimated sky radiance and thus relatively higher SSA. Some of the larger
689 differences between in SSA between OMI and SKYNET, where OMI underestimates SSA relative
690 to the SKYNET, can be attributed to the imperfect calibration applied to the SKYNET sensors.

691 **4.2 POSSIBLE SOURCES OF UNCERTAINTIES IN OMAERUV RETRIEVALS**

692 Like other satellite-based remote sensing algorithms, OMAERUV also relies on assumptions
693 about the atmospheric and surface properties for the retrieval of aerosol properties. The single
694 largest known source of error in the OMI retrievals is the subpixel cloud contamination within
695 the OMI footprint. Given the footprint of size $13 \times 24 \text{ km}^2$ for near-nadir pixels which intercept
696 an area of about 338 km^2 on the ground, the presence of subpixel clouds may not be avoided
697 entirely. Currently, the algorithm assigns quality flags to each pixel which carries information on
698 the quality of the retrieval depending upon the observed conditions (*Torres et al.*, 2013).
699 Aerosol retrieval with the quality flag '0' are considered to be the best in accuracy as this
700 category of flag scheme largely avoids cloud-contaminated pixels by choosing the appropriate
701 thresholds in reflectivity and UVAI measurements.

702

703 Over the desert regions, e.g., the *Dunhuang* SKYNET site in China, the frequency of occurrence
704 of clouds is expected to be minimal. Therefore, it is less likely that the SSA retrievals over these

705 sites are affected by cloud contamination. A reasonable agreement between the two retrieval
706 datasets (Figure 3) supports this assumption. The quality flag scheme, however, cannot
707 entirely rule out the presence of small levels of subpixel cloud contamination or the presence of
708 thin cirrus in the OMI footprint, which can cause overestimation in the retrieval of SSA, such as
709 noted over the SKYNET sites in *Kasuga, Etchujima, Seoul, Bologna, and Pune*. Largest
710 uncertainties observed over these sites are associated with the urban-industrial aerosol type,
711 possibly due to the fact that the AOD's for this aerosol type are the lowest in the analysis, and
712 therefore, subject to the less sensitivity to absorption and possibly more affected by sub-pixel
713 cloud contamination.

714
715 Another possible source of uncertainty can be the assumption of the aerosol layer height. The
716 climatology of aerosol layer height derived from CALIOP measurements adequately describes
717 the observed mean layer of carbonaceous and desert dust aerosols (*Torres et al., 2013*). It is
718 particularly robust over the arid and semiarid areas where large numbers of cloud-free
719 observations were used in the calculation. However, note that the temporal and spatial
720 coverage of CALIOP is limited to 16-day repeat cycle over the same location. Variations in the
721 aerosol layer height not observed by CALIOP, therefore, will be missed out in the derived
722 climatology and thus can be a source of uncertainty. Sensitivity analysis of the OMAERUV
723 retrievals suggests that an overestimation (underestimation) in the aerosol layer height results
724 in an overestimated (underestimated) SSA. ~~This is because an increase (decrease) in the aerosol~~
725 ~~layer height from the actual one enhances (reduces) absorption signal in the radiance~~
726 ~~measurements in near-UV, which the OMAERUV algorithm compensates by retrieving higher~~
727 ~~AOD and SSA to match with the observations.~~ This is because an increase (decrease) in the
728 assumed aerosol layer height from the actual one enhances (reduces) absorption in the
729 radiance look-up table (not in the actual TOA measurements), which the OMAERUV algorithm
730 compensates by retrieving lower (higher) AOD and higher (lower) SSA to match with the
731 observations.

732

733 The third source of uncertainty that can affect SSA retrieval is the accuracy of the prescribed
734 surface albedo. For the surface characterization, the OMAERUV algorithm use a near-UV
735 surface albedo database derived using the multiyear OMI reflectivity observations. The method
736 adopts a minimum reflectivity approach, ensuring minimal or no contamination from the
737 atmosphere, i.e., aerosols and clouds, in the measurements. Afterward, the minimum
738 reflectivity dataset derived from the OMI observations was adjusted in the temporal domain to
739 the seasonality of surface albedo retrieved in the visible wavelengths from MODIS. The dataset
740 contains surface albedo values at 354 and 388 nm at a grid resolution of $0.25^\circ \times 0.25^\circ$.
741 Compared to the previous OMAERUV dataset using TOMS-based surface albedo product at 1°
742 grid resolution, the new OMI-based dataset is expected to be more accurate to within 0.005 to
743 0.01 owing to its higher spatial resolution and the fact that it is contemporary to the OMI
744 operation. A sensitivity study of the OMAERUV retrievals to the change in surface albedo
745 described in *Jethva et al. (2014)* suggests that an increase in surface albedo by 0.01 in the near-
746 UV region over desert areas results in a decrease in the magnitude of retrieved SSA by ~ -0.02 .
747 The effect of uncertain surface albedo can be more pronounced at lower aerosol loading,
748 where the reduced signal from the atmosphere makes OMAERUV retrieval more susceptible to
749 the uncertainty in surface albedo.

750

751 The assumed aerosol microphysical and optical properties could be additional sources of
752 uncertainty. The particle size distributions assumed in the OMAERUV models are adopted from
753 long-term AERONET inversion statistics (*Dubovik et al., 2002*), representing areas influenced by
754 smoke, dust, and urban/industrial aerosols, and therefore are considered realistic
755 representations of the total atmospheric column. The carbonaceous smoke aerosols are
756 assumed to be spherical in shape with a bimodal log-normal size distribution and characterized
757 with a steep absorption gradient, such that the Absorption Angstrom Exponent (AAE) in the
758 near-UV lies in the range 2.5-3.0, to adequately represent the organics in the biomass burning
759 smoke particles (*Kirchstetter et al., 2004; Jethva and Torres, 2011*). The desert dust aerosol
760 model follows bimodal log-normal size distribution with particles comprised of randomly
761 oriented spheroids with an axis ratio (shape factor) distribution adopted from *Dubovik et al.*

762 (2006). The sensitivity study followed by an actual inversion of OMI data presented in Torres et
763 al. (2018) demonstrates that the change in dust particle shape from spherical to spheroidal
764 distribution improved the AOD retrievals significantly and brought the equivalency between the
765 retrievals over left and right sides of the OMI swath for the dust belt region of tropical Atlantic.
766 The associated changes in SSA retrievals were noted within ± 0.01 and -0.02 for the scattering
767 angle up to 100° - 150° and $>160^\circ$, respectively. The OMAERUV version 1.8.9.1 data product used
768 in the present study adopts spheroidal dust model based on the work of Dubovik et al. (2006)
769 and Torres et al. (2018). The spectral dependence of the refractive index in the near-UV
770 assumed in the dust aerosol model is generally consistent with the in-situ laboratory
771 measurements (*Wagner et al.*, 2012). For instance, retrieval of AOD and SSA for carbonaceous
772 aerosols using the smoke model with AAE of 1.90 (10% relative spectral dependence in the
773 imaginary index between 354 and 388 nm) and 1.0 (no spectral dependence in the imaginary
774 index), instead of the standard AAE assumption of 2.7, results in a decrease in SSA up to -0.07,
775 respectively, suggesting a marked sensitivity of the SSA retrieval to the significant changes in
776 the spectral aerosol absorption. Due to the shortage of ground-based characterization of
777 absorption in the near-UV part of the spectrum, the regional representation of the spectral
778 absorption properties in the OMAERUV models is limited. Therefore, spatial and temporal
779 variations in the spectral properties of actual aerosols~~spectral properties~~ can be a potential
780 source of error in the SSA retrieval.

781

782 5 SUMMARY AND CONCLUSION

783 We presented a comparative analysis of the aerosol SSA retrieved from the OMI's two-channel
784 aerosol algorithm (OMAERUV) against an independent ground-based inversion made by the
785 SKYNET Sun photometers over selected 25 sites located mainly in Asia and Europe. This study
786 follows our previous efforts of evaluating the OMI near-UV SSA product carried out using
787 ground-based AERONET dataset (*Jethva et al.*, 2014). The capability of SKYNET sensors to
788 measure the Sun and sky radiance at near-UV wavelengths (340-380-400 nm), and
789 subsequently retrieve the aerosol optical properties, including SSA, at these wavelengths

790 provide a unique opportunity to directly compare the two near-UV SSA products from ground
791 and satellite. Ground-based inversion of SSA at the near-UV wavelengths eliminates the need to
792 adjust and extrapolate satellite retrieval to the visible wavelengths such as the case with
793 comparison against AERONET. Since the SSA inferred from two different platforms are
794 essentially retrieved from two fundamentally different inversion algorithms, the present study
795 does not stand as a “validation” exercise for either retrieval data sets. Instead, the purpose of
796 this analysis was to check the consistency (or lack thereof) between the two retrieved
797 quantities of the same physical parameter regarding standard statistical comparison, i.e., RMSD
798 and % of matchups within the expected uncertainties.

799

800 Unlike AERONET Level 2 inversion product that reports spectral SSA when AOD (440 nm)
801 exceeds a value of 0.4, SKYNET Level 2 dataset delivers spectral SSA in the near-UV and visible
802 parts of the spectrum under all cloud-free observations for all AOD conditions. The collocation
803 procedure that matched temporal inversion data from SKYNET with spatial retrievals from OMI
804 gave resulted in a total of 2691 collocated data points for AOD>0.0 and 1223 when AOD>0.3
805 collected from 25 sites representing biomass burning region of Southeast Asia, desert in China,
806 and urban/industrial areas in Japan, India, and Europe. Combinedly for all 25 sites and under all
807 AOD conditions, we find 38% and 59% of the total SKYNET-OMI SSA agree within their
808 estimated uncertainty range of ± 0.03 and ± 0.05 , respectively, with an overall root-mean-
809 square-difference of 0.06. When restricted with condition AOD>0.3 in both measurements, the
810 agreement of comparison improved to 51% and 72% with root-mean-square-difference of
811 0.047. When segregated by aerosol type, the agreement between the two sensors is found to
812 be robust for matchups identified as the carbonaceous aerosols over several sites in Japan,
813 *Seoul* in South Korea, *Phimai* in Thailand, and *New Delhi* in India, yielding 61% and 84% of data
814 points falling within the limits of ± 0.03 and ± 0.05 with an overall RMSD of 0.035. The
815 collocation procedure found few matchups for desert dust aerosol, mostly over *Dunhuang* site
816 in China, showing a reasonable comparison with 50% and 68% data points within expected
817 uncertainty limits. Among the three major aerosol types, the urban/industrial type aerosols

818 provide the maximum number of matchup data points with a relatively poorer comparison,
819 where 45% and 67% data are found to be within the uncertainty limits.

820

821 The differences in SSA between OMI and SKYNET are found to be larger~~st~~ at lower aerosol
822 loading, where OMI retrieves significantly higher SSA compared to that of SKYNET. However,
823 the differences are minimized at larger AOD values (>0.5) suggesting a convergence in both
824 retrievals at moderate to larger~~r~~ aerosol loading. Similarly, the differences in SSA exhibit a
825 stronger relationship to UVAI showing larger discrepancies beyond expected uncertainty limits
826 at lower UVAIs (<0), but nearing to zero with a reduced spread in matchups at larger
827 magnitudes of UVAI (>0.2-0.3).

828

829 Much of the inconsistency observed between OMI and SKYNET at lower aerosol loadings
830 indicate retrieval issues due to reduced signal-to-noise ratio and uncertain algorithmic
831 assumptions. For instance, the OMAERUV retrievals are more susceptible to the changes in
832 surface albedo at lower AODs, and to the spectral absorption at higher AODs (*Torres and Jethva,*
833 2011). On the other hand, the SKYNET inversion algorithm assumes a wavelength-independent
834 surface albedo of 0.1 across the UV to visible-near-IR wavelengths, which appears to be
835 unrealistic especially in the UV region where OMI surface albedo dataset shows much lower
836 values (<0.05) over land. Though the reflected light from surface plays a second-order role in
837 the ground-based retrievals, previous studies as well as shown in the present work (Figure 68),
838 uncertainty in surface albedo can cause non-negligible errors in SSA retrievals that likely exceed
839 the expected accuracy level of ± 0.03 .

840

841 Despite the inherent uncertainties associated with both satellite and ground inversion products,
842 a good level of agreement between the two independent techniques over SKYNET sites at
843 increasing aerosol loading is encouraging. We intend to extend the present analysis to other
844 SKYNET sites whose data are still not directly accessible in the public domain. Continuing the

845 evaluation of inversion products, both from satellite and ground, is an important exercise to
846 track the changes and improvements in the algorithms and resulting data products, and to
847 establish the consistency (or lack thereof) that can help to diagnose further and improve the
848 accuracy of retrievals.

849

850 **ACKNOWLEDGMENTS**

851 We thank the Center for Environmental Remote Sensing (CERes), Chiba University, Japan
852 (<http://atmos3.cr.chiba-u.jp/skynet/data.html>), for the online availability of the SKYNET dataset
853 for several sites in Japan, South Korea, China, India, Italy, and Germany. Acknowledgments are
854 also due to the principal investigators and their staff for establishing and maintaining respective
855 SKYNET sites, whose data are used in the present work. We acknowledge the support of NASA
856 GES-DISC, the NASA Earth Science data center, for the online availability of the OMI aerosol
857 product assessed in this analysis. Thanks are due to the two anonymous reviewers for offering
858 constructive comments leading to the improvements in the article.

859 AUTHORS' CONTRIBUTIONS

860 Dr. Jethva, the leading author, conceptualized the study and wrote the paper. He conducted
861 comparative data analysis of OMI- and SKYNET-retrieved single-scattering albedo products
862 presented in the paper. Dr. Torres (2nd author) brought his expertise in interpreting the results
863 and helped improving the manuscript writeup.

864

865 Additional Information

866 The author(s) declare no competing interests, financial or non-financial.

867 **REFERENCES**

- 868 Ahn, C., O. Torres, and P. K. Bhartia: Comparison of Ozone Monitoring Instrument UVAerosol
869 Products with Aqua/Moderate Resolution Imaging Spectroradiometer and Multiangle Imaging
870 Spectroradiometer observations in 2006, *J. Geophys. Res.*, 113, D16S27,
871 doi:10.1029/2007JD008832, 2008.
- 872
- 873 Ahn, C., O. Torres, and H. Jethva: Assessment of OMI near-UV aerosol optical depth over land, *J.*
874 *Geophys. Res. Atmos.*, 119, doi:10.1002/2013JD020188, 2014.
- 875
- 876 Boi, P., G. Tonna, G. Dalu, T. Nakajima, B. Olivieri, A. Pompei, M. Campanelli, and R. Rao:
877 Calibration and data elaboration procedure for sky irradiance measurements, *Appl. Opt.*, 38,
878 896-907, 1999.d
- 879
- 880 Campanelli, M., T. Nakajima, B. Olivieri: Determination of the solar calibration constant for a
881 sun-sky radiometer, *Applied Optics*, 43(3), 2004.
- 882
- 883 Campanelli, M., G. Gobbi, C. Tomasi, and T. Nakajima: Intercomparison between aerosol
884 characteristics retrieved simultaneously with a Cimel and Prede Sun-sky radiometers in Rome
885 (TorVergata AERONET site), *Opt. Pura Apl.*, 37, 3159–3164, 2004a.
- 886
- 887 Campanelli, M., V. Estelles, C. Tomasi, T. Nakajima, V. Malvestuto and J. A. Martinez-Lozan:
888 Application of the SKYRAD improved Langley plot method for the in situ calibration of CIMEL
889 sun-sky photometers, *Applied Optics*, 46(14), 2007.
- 890
- 891 [Campanelli, M., Estellés, V., Colwell, S., Shanklin, J., and Ningombam S. S.: Analysis of aerosol](#)
892 [optical properties from continuous sun-sky radiometer measurements at Halley and Rothera,](#)
893 [Antarctica over seven years, *Geophysical Research Abstracts*, Vol. 17, EGU2015-2768, EGU](#)
894 [General Assembly, 2015.](#)
- 895
- 896 Campanelli, M., A. M. Iannarelli, S. Kazadzis, N. Kouremeti, S. Vergari, V. Estelles, H. Diemoz, A.
897 di Sarra, A. Cede: The QUATRAM Campaign: QUALity and TRaceability of Atmospheric aerosol
898 Measurements, The 2018 WMO/CIMO Technical Conference on Meteorological and
899 Environmental Instruments and Methods of Observation (CIMO TECO-2018) “Towards fit-for-
900 purpose environmental measurements”, 2018.
- 901

- 902 Che, H., G. Shi, A. Uchiyama, A. Yamazaki, H. Chen, P. Goloub, and X. Zhang: Intercomparison
903 between aerosol optical properties by a PREDE skyradiometer and CIMEL sunphotometer over
904 Beijing, China, *Atmos. Chem. Phys.*, 8, 3199-3214, doi:10.5194/acp-8-3199-2008, 2008.
905
906
- 907 Dubovik, O., A. Smirnov, B. N. Holben, M. D. King, Y. J. Kaufman, T. F. Eck, and I. Slutsker,
908 Accuracy assessments of aerosol optical properties retrieved from Aerosol Robotic Network
909 (AERONET) Sun and sky radiance measurements, *J. Geophys. Res.*, 105(D8), 9791-9806,
910 doi:10.1029/2000JD900040, 2000.
911
- 912 Dubovik, O., B. N. Holben, T. F. Eck, A. Smirnov, Y. J. Kaufman, M. D. King, D. Tanre, and I.
913 Slutsker: Variability of absorption and optical properties of key aerosol types observed in
914 worldwide locations, *J. Atmos. Sci.*, 59, 590–608, 2002.
915
- 916 Dubovik, O., Sinyuk, A., Lapyonok, T., Holben, B. N., Mishchenko, M., Yang, P., Eck, T. F., Volten,
917 H., Munoz, O., Vehelmann, B., van der Zande, W. J., Leon, J. F., Sorokin, M., and Slutsker, I.:
918 Application of spheroid models to account for aerosol particle nonsphericity in remote sensing
919 of desert dust, *J. Geophys. Res.*, 111, D11208, <https://doi.org/10.1029/2005JD006619>, 2006.
920
- 921 Estellés, V., Campanelli, M., Smyth, T. J., Utrillas, M. P., and Martínez-Lozano, J. A.: Evaluation of
922 the new ESR network software for the retrieval of direct sun products from CIMEL CE318 and
923 PREDE POM01 sun-sky radiometers, *Atmos. Chem. Phys.*, 12, 11619-11630,
924 <https://doi.org/10.5194/acp-12-11619-2012>, 2012a.
925
- 926 Estellés, V., Campanelli, M., Utrillas, M. P., Expósito, F., and Martínez-Lozano, J. A.: Comparison
927 of AERONET and SKYRAD4.2 inversion products retrieved from a Cimel CE318 sunphotometer,
928 *Atmos. Meas. Tech.*, 5, 569-579, <https://doi.org/10.5194/amt-5-569-2012>, 2012b.
929
- 930 Estelles, V., N. Kouremeti, M. Campanelli, J. Grobner, J.A. Mari nez-Lozano, S. Kazadzis:
931 Preliminary aerosol optical depth comparison between ESR/SKYNET, AERONET and GAW
932 international networks. International SKYNET workshop, Rome (Italy), 2016.
933
- 934 Khatri, P., and T. Takamura: An algorithm to screen cloud affected data for sky radiometer data
935 analysis, *J. Meteor. Soc. Japan*, 87, 189-204, 2009.
936
- 937 Khatri, P., T. Takamura, A. Yamazaki, and Y. Kondo: Reterival of key aerosol optical parameters
938 for spectral direct and diffuse irradiances measured by a horizontal surface detector, *J. Atmos.*
939 *Oceanic Technol.*, 29, 683–696, 2012.

940
941 Khatri, P., T. Takamura, T. Nakajima, V. Estellés, H. Irie, H. Kuze, M. Campanelli, A. Sinyuk, S.-M.
942 Lee, B. J. Sohn, G. Pandithurai, S.-W. Kim, S. C. Yoon, J. A. Martinez-Lozano, M. Hashimoto, P. C.
943 S. Devara, and N. Manago: Factors for inconsistent aerosol single scattering albedo between
944 SKYNET and AERONET, *J. Geophys. Res. Atmos.*, 121, 1859-1877, doi:10.1002/2015JD023976,
945 2016.
946
947 Kirchstetter, T. W., T. Novakov, and P. V. Hobbs: Evidence that the spectral dependence of light
948 absorption by aerosols is affected by organic carbon, *J. Geophys. Res.*, 109, D21208,
949 doi:10.1029/2004JD004999, 2004.
950
951 Hansen, J., M. Sato, and R. Ruedy: Radiative forcing and climate response, *J. Geophys. Res.*,
952 102(D6), 6831-6864, doi:10.1029/96JD03436, 1997.
953
954
955 Hashimoto, M., Nakajima, T., Dubovik, O., Campanelli, M., Che, H., Khatri, P., Takamura, T., and
956 Pandithurai, G.: Development of a new data-processing method for SKYNET sky radiometer
957 observations, *Atmos. Meas. Tech.*, 5, 2723-2737, <https://doi.org/10.5194/amt-5-2723-2012>,
958 2012.
959
960 IPCC, 2013: Climate Change 2013: The Physical Science Basis. Contribution of Working Group I
961 to the Fifth Assessment Report of the Intergovernmental Panel on Climate Change (Stocker, T.F.,
962 D. Qin, G.-K. Plattner, M. Tignor, S.K. Allen, J. Boschung, A. Nauels, Y. Xia, V. Bex and P.M.
963 Midgley (eds.)). Cambridge University Press, Cambridge, United Kingdom and New York, NY,
964 USA, 1535 pp, doi:10.1017/CBO9781107415324.
965
966 Jethva, H., and O. Torres: Satellite-based evidence of wavelength-dependent aerosol absorption
967 in biomass burning smoke inferred from Ozone Monitoring Instrument, *Atmos. Chem. Phys.*, 11,
968 10,541–10,551, doi:10.5194/acp-11-10541-2011, 2011.
969
970 Jethva, H., O. Torres, and C. Ahn: Global assessment of OMI aerosol single-scattering albedo
971 using ground-based AERONET inversion, *J. Geophys. Res. Atmos.*, 119,
972 doi:10.1002/2014JD021672, 2014.
973
974 Mok, J., Krotkov, N. A., Torres, O., Jethva, H., Li, Z., Kim, J., Koo, J.-H., Go, S., Irie, H., Labow, G.,
975 Eck, T. F., Holben, B. N., Herman, J., Loughman, R. P., Spinei, E., Lee, S. S., Khatri, P., and
976 Campanelli, M.: Comparisons of spectral aerosol single scattering albedo in Seoul, South Korea,
977 *Atmos. Meas. Tech.*, 11, 2295-2311, <https://doi.org/10.5194/amt-11-2295-2018>, 2018.

- 978
979 Nakajima, T., G. Tonna, R. Rao, P. Boi, Y. Kaufman, and B. Holben: Use of sky brightness
980 measurements from ground for remote sensing of particulate polydispersions, *Appl. Opt.*, 35,
981 15, 2672-2686, 1996.
- 982
983 Schenkeveld, V. M. E., Jaross, G., Marchenko, S., Haffner, D., Kleipool, Q. L., Rozemeijer, N. C.,
984 Veefkind, J. P., and Levelt, P. F.: In-flight performance of the Ozone Monitoring Instrument,
985 *Atmos. Meas. Tech.*, 10, 1957–1986, <https://doi.org/10.5194/amt-10-1957-2017>, 2017.
- 986
987 Torres, O., P. K. Bhartia, J. R. Herman, Z. Ahmad, and J. Gleason: Derivation of aerosol
988 properties from satellite measurements of backscattered ultraviolet radiation: Theoretical basis,
989 *J. Geophys. Res.*, 103(D14), 17,099–17,110, doi:10.1029/98JD00900, 1998.
- 990 Torres, O., P. K. Bhartia, A. Sinyuk, E. J. Welton, and B. Holben: Total Ozone Mapping
991 Spectrometer measurements of aerosol absorption from space: Comparison to SAFARI 2000
992 ground-based observations, *J. Geophys. Res.*, 110, D10S18, doi:10.1029/2004JD004611, 2005
- 993
994 Torres, O., A. Tanskanen, B. Veihelmann, C. Ahn, R. Braak, P. K. Bhartia, P. Veefkind, and P.
995 Levelt: Aerosols and surface UV products from Ozone Monitoring Instrument observations: An
996 overview, *J. Geophys. Res.*, 112, D24S47, doi:10.1029/2007JD008809, 2007.
- 997 Torres, O., C. Ahn, and Z. Chen: Improvements to the OMI near-UV aerosol algorithm using A-
998 train CALIOP and AIRS observations, *Atmos. Meas. Tech.*, 6, 3257–3270, doi:10.5194/amt-6-
999 3257-2013, 2013.
- 1000 Torres, O., Bhartia, P. K., Jethva, H., and Ahn, C.: Impact of the ozone monitoring instrument
1001 row anomaly on the long-term record of aerosol products, *Atmos. Meas. Tech.*, 11, 2701-2715,
1002 <https://doi.org/10.5194/amt-11-2701-2018>, 2018.
- 1003 Wagner, R., T. Ajtai, K. Kandler, K. Lieke, C. Linke, T. Müller, M. Schnaiter, and M. Vragel:
1004 Complex refractive indices of Saharan dust samples at visible and near UV wavelengths: A
1005 laboratory study, *Atmos. Chem. Phys.*, 12, 2491–2512, doi:10.5194/acp-12-2491-2012, 2012.
- 1006

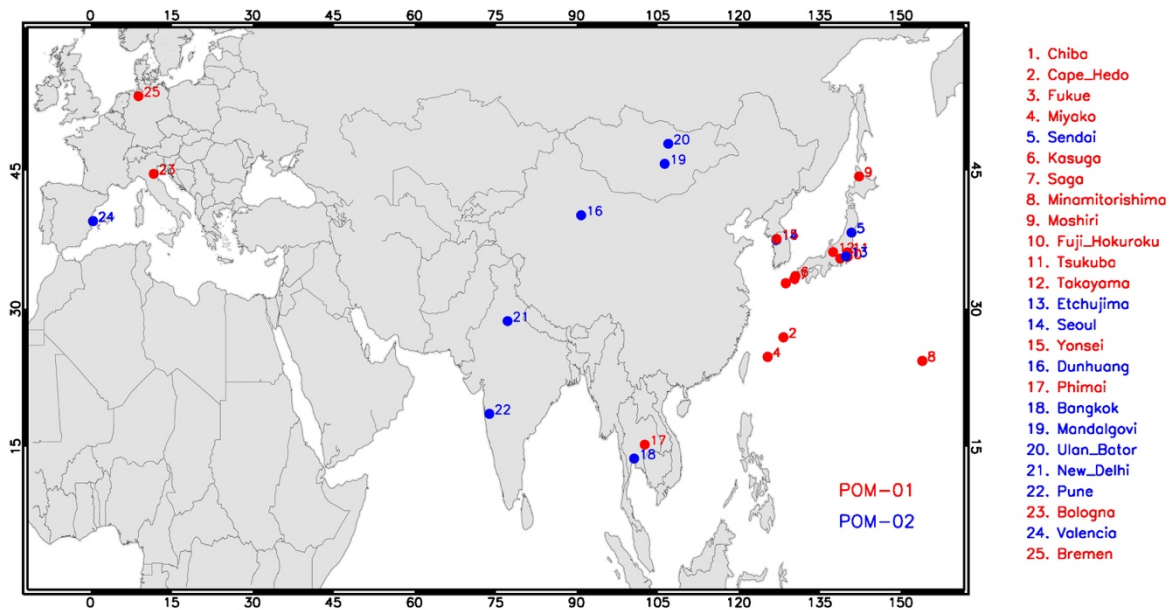
1007 **TABLES**

1008 *Table 1 A list of SKYNET sites and corresponding dataset used in the present analysis. Sensor*
 1009 *type “POM02” consists of a total of seven wavelength filters, including near-UV bands, i.e., 340,*
 1010 *380, 400, 500, 675, 870, and 1020 nm, whereas “POM01” sensors have a total of five*
 1011 *wavelength filters, i.e., 400, 500, 675, 870, and 1020 nm. The rightmost four columns enlist the*
 1012 *statistical measures of OMI-SKYNET single-scattering albedo matchups.*

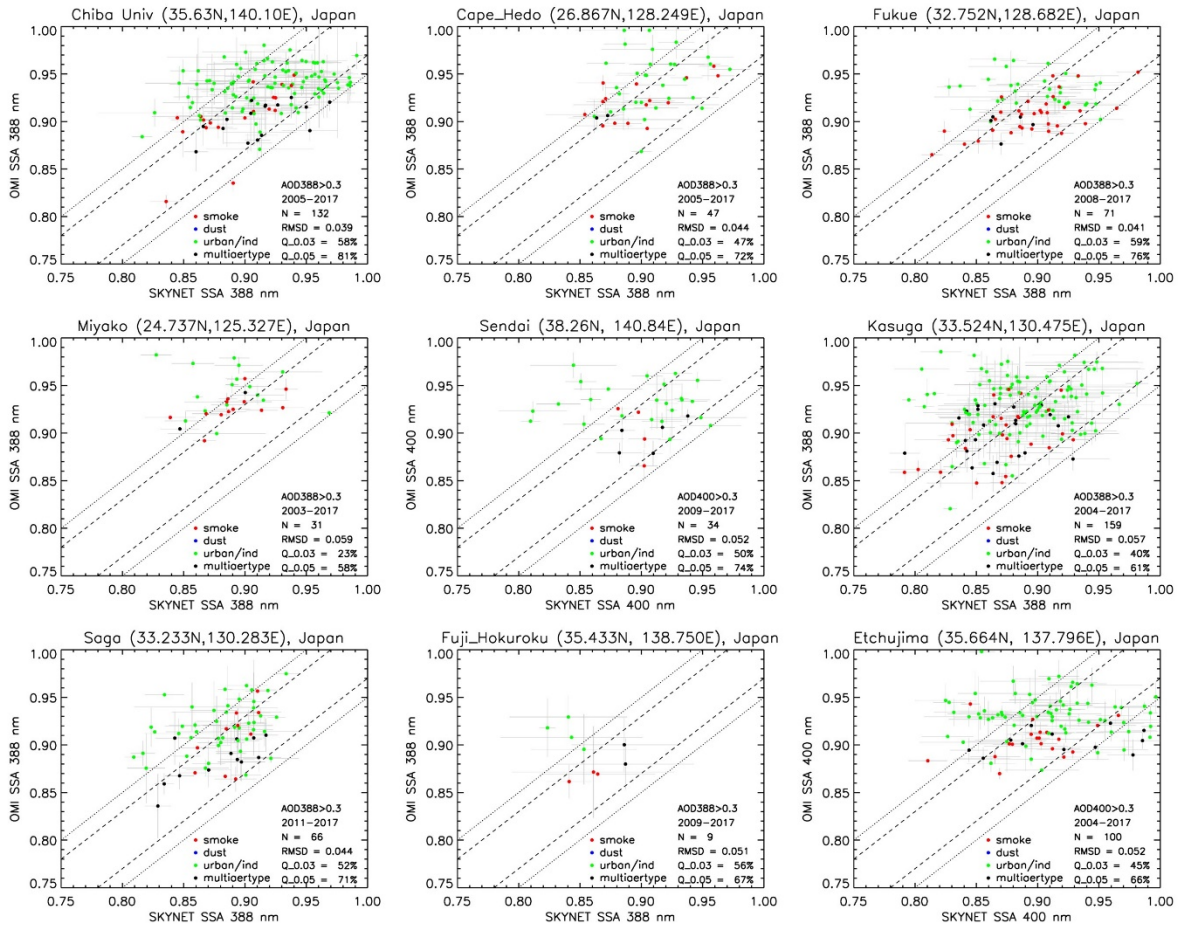
1013 *Abbreviations: N: number of satellite-ground matchups, RMSD: root-mean-square-difference between OMI and*
 1014 *SKYNET, Q_{0.03} and Q_{0.05}: percent matchups within an absolute difference of 0.03 and 0.05.*

SKYNET Station Name	Longitude	Latitude	Country	Sensor Type	Data Period	N	RMSD	Q _{0.03} (%)	Q _{0.05} (%)
<i>Chiba University</i>	140.104°E	35.625°N	Japan	POM02	2005-2017	132	0.039	58	81
<i>Cape Hedo</i>	128.248E	26.867N	Japan	POM02	2005-2017	47	0.044	47	72
<i>Fukue</i>	128.682E	32.752N	Japan	POM02	2008-2017	71	0.041	59	76
<i>Miyako</i>	125.327E	24.737N	Japan	POM02	2004-2017	31	0.059	23	58
<i>Sendai</i>	140.84E	38.26N	Japan	POM01	2009-2017	34	0.052	50	74
<i>Kasuga</i>	130.475E	33.524N	Japan	POM02	2004-2017	159	0.057	40	61
<i>Saga</i>	130.283E	33.233N	Japan	POM02	2011-2017	66	0.044	52	71
<i>Minamitorishima</i>	153.97E	24.3N	Japan	POM02	2006-2009	-	-	-	-
<i>Moshiri</i>	142.260E	44.366N	Japan	POM02	2009-2011	2	0.018	100	100
<i>Fuji Hokuroku</i>	138.750E	35.433N	Japan	POM02	2009-2017	9	0.051	56	67
<i>Tsukuba</i>	140.096E	36.114N	Japan	POM02	2014-2017	5	0.027	80	100
<i>Takayama</i>	137.423E	36.145N	Japan	POM02	2014-2017	3	0.022	67	100
<i>Etchujima</i>	139.796E	35.664N	Japan	POM01	2004-2010	100	0.052	45	66
<i>Seoul</i>	126.95E	37.46N	Republic of South Korea	POM01	2005-2015	182	0.050	42	66
<i>Yonsei</i>	126.980E	37.570N	Republic of South Korea	POM02	2016	5	0.035	40	80
<i>Dunhuang</i>	90.799E	40.146N	China	POM01	1999-2007	40	0.048	50	68
<i>Phimai</i>	102.564E	15.184N	Thailand	POM02	2005-2017	139	0.031	71	91
<i>Bangkok</i>	100.605E	13.667N	Thailand	POM02	2009-2017	15	0.064	47	60
<i>Mandalgovi</i>	106.264E	45.743N	Mongolia	POM01	1998-2009	4	0.087	0	0
<i>Ulan Bator</i>	106.921E	47.923N	Mongolia	POM01	2013-2017	2	0.026	100	100
<i>New Delhi</i>	77.174E	28.629N	India	POM01	2006-2007	63	0.038	52	83
<i>Pune</i>	73.805E	18.537N	India	POM01	2004-2009	94	0.050	39	64
<i>Bologna</i>	11.34E	44.52N	Italy	POM02	2014-2017	114	0.065	25	50
<i>Valencia</i>	0.420E	39.507N	Spain	POM01	2014-2017	4	0.052	25	25
<i>Bremen</i>	8.854E	3.108N	Germany	POM02	2009	-	-	-	-

1015

1016 **FIGURES**

1017
 1018 **Figure 1** Geographical placement of ground-based SKYNET sensors over sites in Asia and Europe
 1019 The SKYNET dataset for these sites are freely accessible from the Center for Environmental
 1020 Remote Sensing (CERes), Chiba University, Japan ([http://atmos3.cr.chiba-](http://atmos3.cr.chiba-u.jp/skyenet/data.html)
 1021 [u.jp/skyenet/data.html](http://atmos3.cr.chiba-u.jp/skyenet/data.html)).



1022

1023

1024

1025

1026

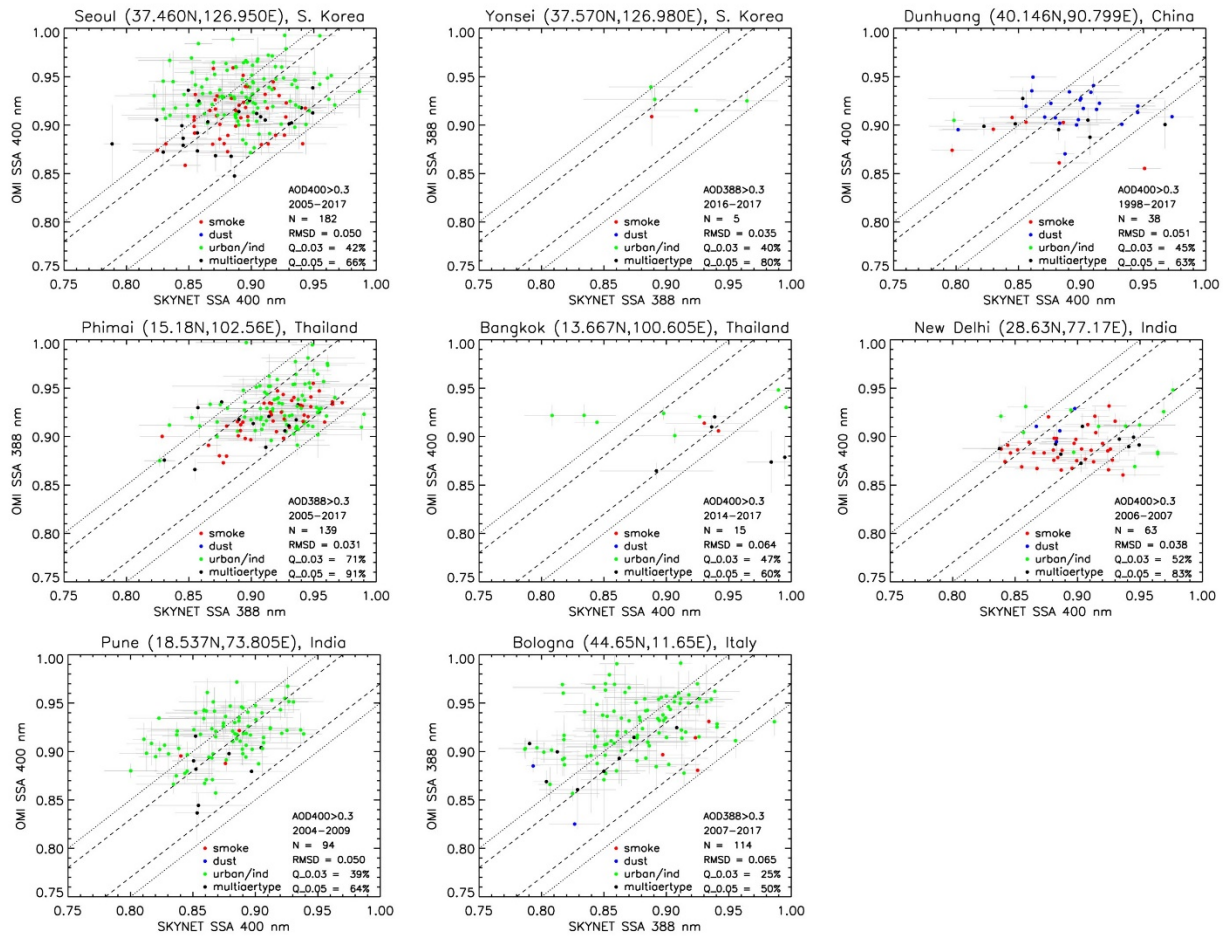
1027

1028

1029

1030

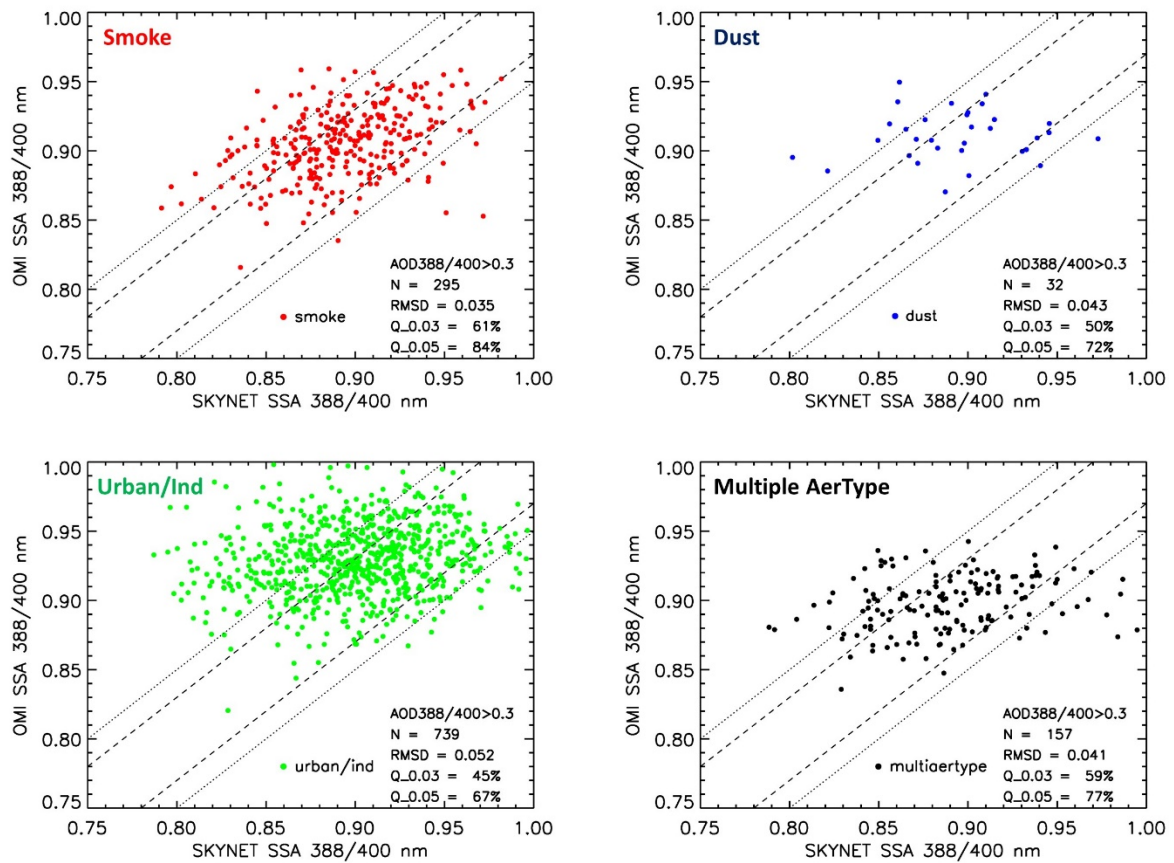
Figure 2 OMAERUV versus SKYNET single-scattering albedo comparison for different sites in Japan. Legends with different colors represent the aerosol type selected by the OMAERUV algorithm for the co-located matchups (N). RMSD is the root-mean-square difference between the two retrievals; Q_0.03 and Q_0.05 are the percents of total matchups (N) that fall within the absolute difference of 0.03 and 0.05, respectively. OMI-SKYNET matchups with AOD>0.3 (388 or 400 nm) in both measurements are used for comparison.



1031

1032 **Figure 3** Same as in Figure 2 but for SKYNET sites in South Korea, China, Thailand, India, and

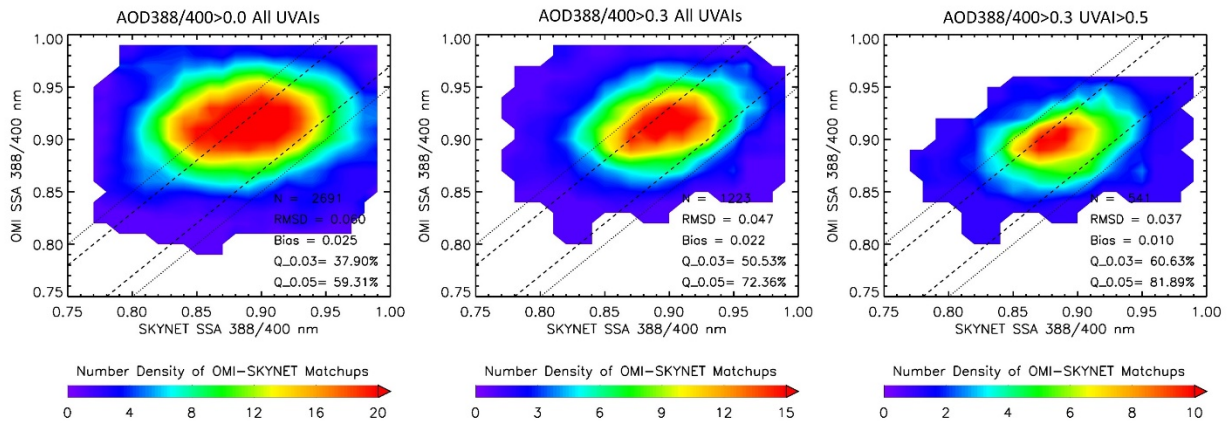
1033 Italy.



1034

1035 **Figure 4** Composite scatterplots of OMAERUV versus SKYNET single-scattering albedo (388 or
 1036 400 nm) for the three distinct aerosol types, i.e., smoke, dust, and urban/industrial, as
 1037 identified by the OMAERUV algorithm. OMI-SKYNET matchups with AOD>0.3 (388 or 400 nm) in
 1038 both measurements are used for the comparison.

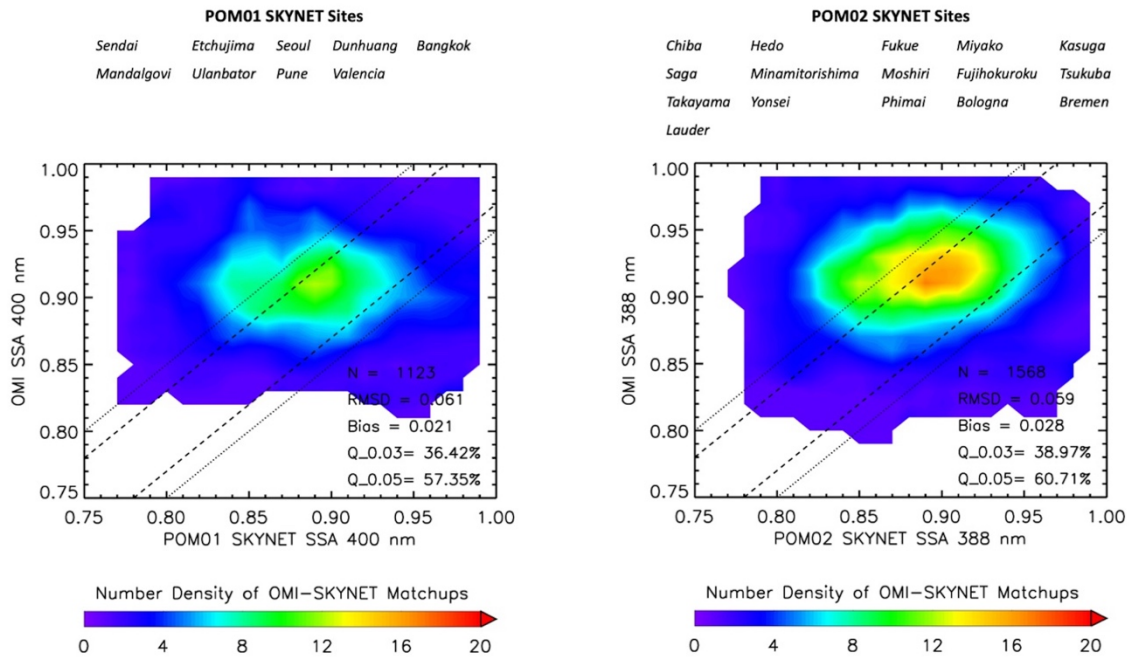
1039



1040

1041 [Figure 5](#) Composite [number density contour](#) plots of SSA comparison between OMI and SKYNET
 1042 [for different aerosol loading conditions](#). The resultant statistics of the comparison are depicted
 1043 [in the lower-right in each plot](#). Note that the scale used for number density of satellite-ground
 1044 [matchups for the three sets of comparisons are different](#).

1045



1046

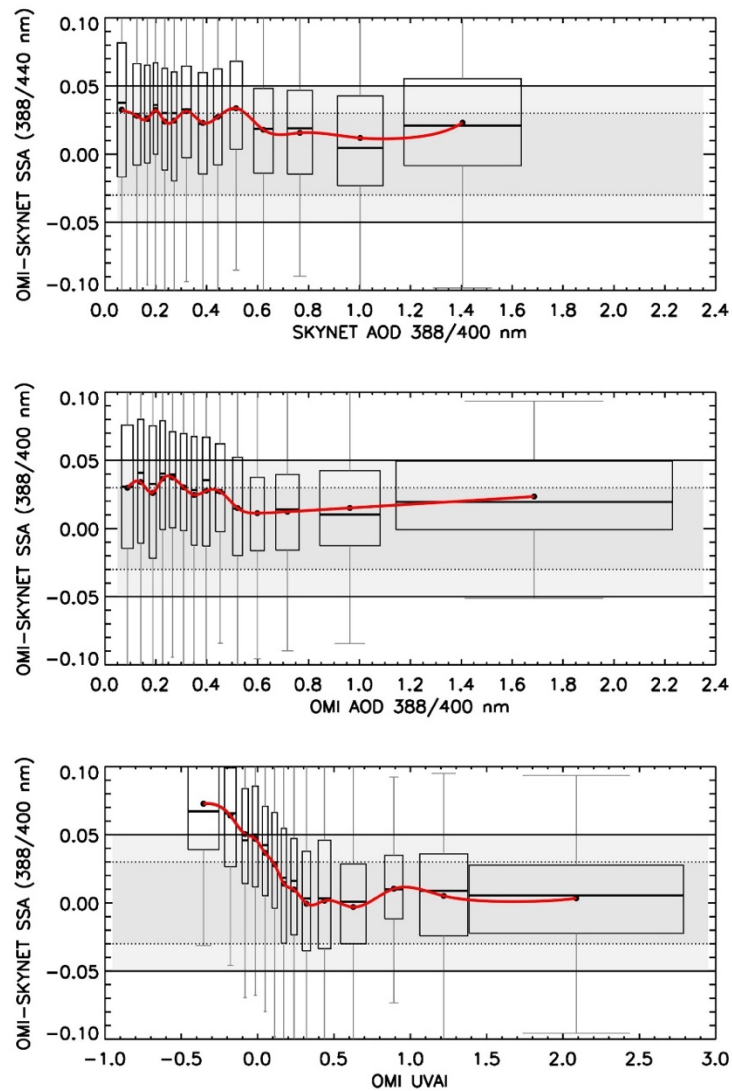
1047

1048

1049

1050

Figure 6 Composite number density contour plots of SSA comparison between OMI and SKYNET for different aerosol loading conditions. The resultant statistics of the comparison are depicted in the lower-right in both plots.



1051

1052

1053

1054

1055

1056

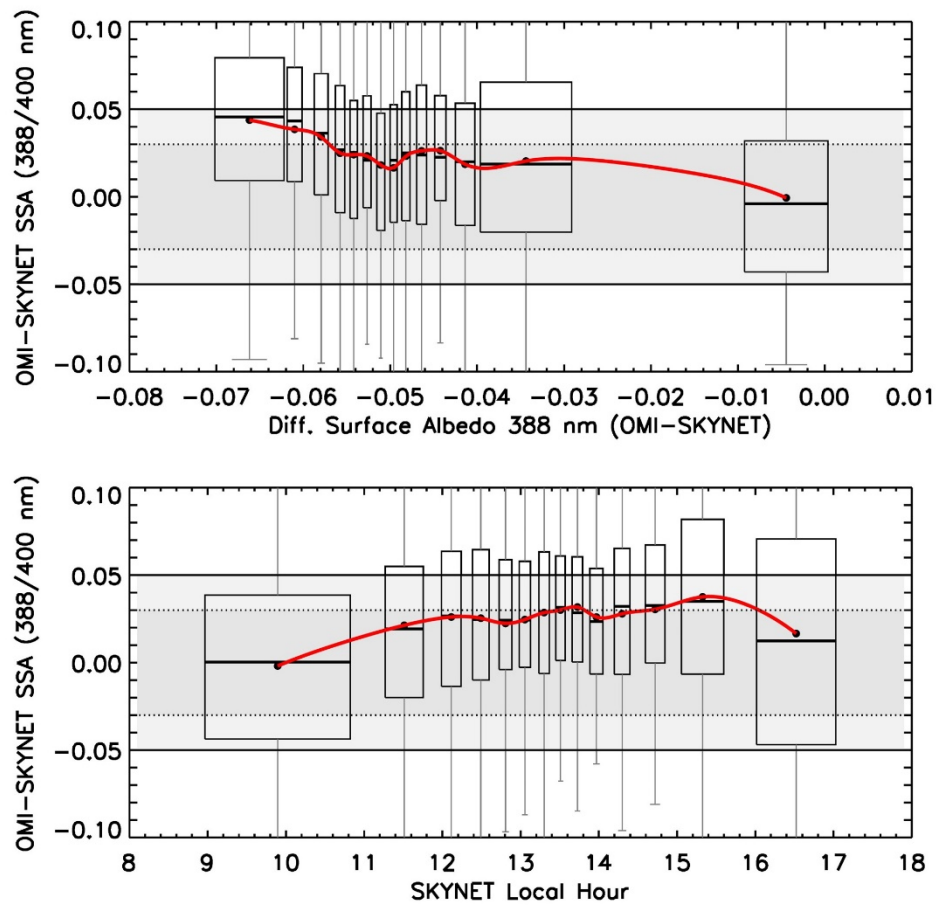
1057

1058

1059

1060

Figure 65.7 Difference in [single-scattering albedo-SSA](#) between OMI and SKYNET as a function of the coincident SKYNET-measured (top panel) and OMI-retrieved (middle panel) aerosol optical depth and OMI-measured UVAI (bottom panel). Filled circles in black are the mean of difference for each AOD and UVAI bin with an equal sample size of [150200](#) matchups; horizontal lines represent median of the bin samples; shaded area in gray encompasses data within 25 (lower) to 75 (higher) percentile range, whereas vertical lines in gray represent 1.5 times inter-quartile range (25 to 75 percentile). The dotted and solid horizontal lines are the uncertainty range of ± 0.03 and ± 0.05 respectively. The width of each box represents 2-standard deviation of the data contained in the respective bins.



1061
1062 **Figure 768** Same as in Figure 75 but the difference in SSA between OMI and SKYNET is related
1063 to (a) the difference in surface albedo assumed by the two algorithms and (b) local
1064 measurement hour of SKYNET.